Aalto University
School of Engineering

Henri Tikkanen

Hydrological modeling of a large urban catchment using a stormwater management model (SWMM)

Master's thesis submitted in partial fulfillment of the requirements for the degree of Master of Science in Technology in the Degree Programme in Transport and Environmental Engineering.

Espoo, 13.08.2013
Supervisor: Professor Harri Koivusalo
Instructor: M.Sc. Gerald Krebs

ABSTRACT

Author Henri Tikkanen

Title of thesis Hydrological modeling of a large urban catchment using a stormwater management model (SWMM)

Degree programme Transport and Environmental Engineering

Major/minor Water and Environmental Engineering / Strategic Management **Code of professorship** Yhd-12

Thesis supervisor Professor Harri Koivusalo

Thesis instructor M.Sc. Gerald Krebs

Date 13.08.2013 **Number of pages** 64+1 **Language** English

Abstract

Stormwater modeling has a major role in preventing issues such as flash floods and urban water-quality problems. However, in-detail modeling of large urban areas is time-consuming as it typically involves model calibration based on highly detailed input data. Stormwater models of a lowered spatial resolution would thus appear valuable if only their ability to provide realistic results could be proved.

This study proposes a methodology for rapid catchment delineation and stormwater management model (SWMM) parameterization in a large urban area, without calibration. The effect of spatial resolution on the accuracy of modeling results is also being discussed.

A catchment delineation and SWMM parameterization is conducted for an urban area in the city of Lahti in southern Finland. GIS methodology is utilized for simultaneous processing of data representing large areas. Literature values are also of importance where no spatial data is available. To evaluate the parameterization results, the SWMM application is run using an hourly data series of meteorological observations covering a period of four years.

The routines established in the study make the catchment delineation and subdivision process reasonably fast and accurate, although manual work cannot be fully avoided due to defects in the input data. In contrast, the SWMM parameterization of the low-resolution subcatchments is the more challenging part and involves larger uncertainties. Even so, the model application provides sufficient results compared to literature and other studies performed on the same site, indicating non-calibrated SWMM applications of low spatial resolution seem promising for certain tasks in stormwater modeling. Overall, the methods developed in this study provide a feasible approach for SWMM parameterization in large urban areas.

Keywords Urban Hydrology; Stormwater; Modeling; SWMM

TIIVISTELMÄ

Tekijä Henri Tikkanen

Diplomityön otsikko Laajan taajama-alueen hydrologinen mallinnus SWMM-hulevesimallilla

Tutkinto-ohjelma Yhdyskunta- ja ympäristötekniikka

Pääaine/Sivuaine Vesi- ja ympäristötekniikka / Strateginen johtaminen **Pääaineen koodi** Yhd-12

Työn valvoja Prof. Harri Koivusalo

Työn ohjaaja M.Sc. Gerald Krebs

Päiväys 13.08.2013 **Sivumäärä** 64+1 **Kieli** Englanti

Tiivistelmä

Hulevesimallinnus on tärkeä työkalu muun muassa taajamatulvien sekä kaupunkivesien laatuongelmien välttämiseksi. Yksityiskohtainen hulevesimallinnus vaatii kuitenkin paljon aikaa, sillä se edellyttää yleensä mallin kalibrointia tarkkojen lähtötietojen perusteella. Tämän vuoksi olisi hyödyllistä, mikäli myös vähemmän hajautettujen hulevesimallien voitaisiin todistaa tuottavan todenmukaisia tuloksia.

Tässä työssä esitetään menetelmiä tehokasta taajamien valuma-alueiden rajaamista ja kalibroimattoman SWMM-hulevesimallin parametrisointia varten. Myös hulevesimallien maantieteellisen resoluution merkitystä tarkastellaan.

Lahden kaupungin keskusta-alueelle tehdään valuma-aluejako sekä SWMM-hulevesimallin (stormwater management model) parametrisointi. Laajoja alueita koskevan tiedon käsittelemiseen kerralla käytetään paikkatietomenetelmiä. Myös kirjallisuusarvoja hyödynnetään niiltä osin, kuin paikkatietoja ei ole saatavilla. Parametrisoinnin tarkistamiseksi SWMM-hulevesimallia sovelletaan käyttäen tunneittaista, neljän vuoden jakson kattavaa säähavaintoaineistoa.

Valuma-aluejako ja osavaluma-aluejako voidaan tehdä työssä kehitetyillä menetelmillä nopeasti ja tarkasti, vaikkakaan prosessia ei voida kokonaan automatisoida lähtöaineistojen epätäydellisyyden vuoksi. Toisaalta osavaluma-alueiden parametrisointi on haastavaa ja sisältää suurempia epävarmuuksia kuin valuma-aluejako. Niistäkin huolimatta hulevesimallin sovellus tuottaa järkeviä tuloksia kirjallisuuteen ja muihin samalla alueella tehtyihin tutkimuksiin verrattuna. Tämän perusteella myös kalibroimaton, pienen maantieteellisen resoluution SWMM-malli voi olla riittävä joihinkin hulevesimallinnuksen sovelluksiin. Työssä kehitetyt menetelmät tarjoavat kaiken kaikkiaan toimivan tavan laajaa taajama-aluetta kuvaavan SWMM-hulevesimallin parametrisointiin.

Avainsanat Taajamahydrologia; Hulevesi; Mallinnus; SWMM-hulevesimalli

FOREWORD

First, I would like to thank Professor Harri Koivusalo, the supervisor of this study, for being extremely supportive and encouraging throughout my work on this topic. You gave me a clear direction on where to aim.

I would also like to thank my advisor Gerald Krebs (M.Sc.) for all the comments and guidance, as well as every clarifying conversation we had along the way. You were always ready to help.

This study was conducted as a part of the research project *'Urban laboratory for sustainable built environment – Water cycle and ecosystem services in an urban environment'*. The project, mainly funded by the European Regional Development Fund (ERDF), is done in cooperation between Aalto University, the University of Helsinki, and Lahti University of Applied Sciences. Thank you to all the other people working on the project – many of you gave valuable input to my work as well.

Part of this work was also funded by Maa- ja vesitekniikan tuki ry, for which they deserve a special acknowledgement.

Last, the biggest thanks go to my family, and especially Iiris. Through all my studies, you were always there, prompting me to do my best. Thank you!

Espoo, 5.8.2013

Henri Tikkanen

TABLE OF CONTENTS

LIST OF FIGURES

LIST OF TABLES

1. INTRODUCTION

The importance of urban stormwater modeling is constantly increasing due to three global trends: urbanization, population growth, and climate change. The first two trends induce a rapid growth of cities, making stormwater management ever more challenging while at the same time a rising number of people is affected by the harmful effects of stormwater on the environment. In many areas, these effects are expected to be amplified in the future due to climate change and associated higher frequencies of extreme weather events.

Stormwater is water generated on the land surface, originating from rainfall or melting snow or ice (Durrans, 2003). The concept of stormwater is strongly related to urban areas where conveyance systems exist. In Finland, conveyance systems have been typically designed based on a 10-minute rain event that has a return period of two years. Urban floods are thus not uncommon, sometimes causing material damage worth up to tens of millions of euros. (Aaltonen et al., 2008)

Despite flooding, stormwater also is interesting regarding the urban water balance. The expansion of impervious land-cover implies both larger stormwater runoff volumes and peak flows and consequently reduces other components of the hydrologic cycle, e.g. infiltration and evapotranspiration. Moreover, stormwater directly transports harmful substances from urban surfaces into downstream water systems, thus degrading the water quality. (e.g. Scalenghe and Marsan, 2009; Göbel et al., 2007)

Both stormwater quantity and quality issues can be analyzed and tackled with the aid of *stormwater modeling*. There are numerous different stormwater models for such purposes (Zoppou, 2001). Modeling can be conducted at different spatial resolutions by aggregating similar features together or presenting them separately. The accuracy of coarse-scale models is not yet clearly known so one cannot fully trust the results (Ghosh and Hellweger, 2011). Consequently, high-resolution modeling remains the most exact method, but is often not feasible for large geographical areas. Urban catchments are mostly ungauged, preventing model calibration. And even if the catchments were gauged, the numerous calibration parameters would make calibration hard. In addition, spatial data of sufficient resolution and quality is in many cases unavailable. The parameterization of large-scale stormwater models thus remains challenging, requiring the development of new methodologies. (Rodriguez et al., 2005; Merz et al., 2004)

Objectives and scope of the study

This study was part of the project *'Urban laboratory for sustainable built environment – Water cycle and ecosystem services in an urban environment'*. The overall objective of the study was to develop a methodology of catchment delineation and parameterization that would support a large-scale application of SWMM (Stormwater Management Model) (Rossman, 2010) to an urban area. For the reasons stated in the previous

paragraph, successful large-scale SWMM applications would be a powerful tool for solving stormwater issues. Secondarily, the data produced is also going to be utilized in other ongoing hydrological and water quality studies in the same area.

Central research questions of this study were:

- How to perform detailed catchment delineation and surface discretization for SWMM modeling of a large urban area?
- How should aggregated SWMM parameters be acquired for widely heterogeneous subcatchments?
- Is a large-scale, non-calibrated, long-term SWMM modeling approach (i) realistic and (ii) feasible in a large urban area?

To answer these questions, SWMM was applied to a large urban area. Geographic Information Systems (GIS) were utilized to develop a feasible method for defining aggregated values for spatially variable SWMM parameters. In addition, literature values were used where no detailed spatial data on local conditions was available. Esri ArcGIS 10.1 software (Esri, 2012) was used for all GIS operations. Due to its extensive toolboxes and possibilities for data visualization it provided all functionalities needed for this study. All GIS tools mentioned in the text hereafter refer to those of the ArcGIS software. After processing in GIS software, the spatial data was exported into SWMM.

Several SWMM model runs were conducted for different time periods, using the observed long-term hourly precipitation data as model input. Due to the lack of data the developed model was neither calibrated nor validated. The simulation results were compared to results presented by Krebs et al. (2013a; 2013b) in two distinct parts of the study area. In addition, the results were compared to snow depth measurements as well as literature values on the annual urban water balance. Moreover, the relation between the simulated runoff coefficients and the catchment imperviousness was evaluated.

Structure of the paper

Chapter 2 provides background on basic hydrological and hydraulic concepts as well as an introduction to rainfall-runoff modeling. The background section also covers central previous studies related to the research questions.

Chapter 3 presents the methodology of the study by visualizing the research process and showing which methods were applied for each task.

Chapter 4 describes briefly the study site and presents the data sources used.

Chapter 5 presents as a result the methodology created in this study. These results are also being discussed in the same chapter, as that way the reader can more easily follow the discussion related to each branch of the results.

Finally, Chapter 6 draws the concluding remarks on the study and suggests several interesting areas for further research.

2. BACKGROUND

2.1. Basic hydrological and hydraulic concepts

2.1.1. The catchment and the regional water balance

The basic regional unit in most hydrological considerations and modeling is a catchment (alias drainage basin). A catchment is defined as the area contributing to the stream flows at a certain cross section. Catchments are delineated based on the topography of the area. The line from which water might drain to either one of two different catchments is called a divide. Moreover, the stream cross section through which all the runoff exits the catchment is called a pour point. This point can be located in any part of the stream network, depending on the size of the area of interest for the study at hand. (Dingman, 1994)

Traditionally, catchments have been delineated using topographic maps that show contours for the study area. In the last decades, however, digital elevation models (DEMs) have become the main data source used. They can be analyzed with computer software to obtain information on the catchment delineation, slope, and other parameters (Dingman, 1994). This is discussed further in Chapter 5.1.

The catchment is often considered as a system (see Figure 1), consisting of a control volume subject to the regional water-balance equation:

$$P + G_{in} - (Q + ET + G_{out}) = \Delta S \,, \qquad (1)$$

where
P = precipitation [mm d^{-1}],
G_{in} = ground-water inflow [mm d^{-1}],
Q = stream outflow [mm d^{-1}],
ET = evapotranspiration [mm d^{-1}],
G_{out} = ground-water outflow [mm d^{-1}],
ΔS = change of (liquid and solid) water storages [mm d^{-1}].

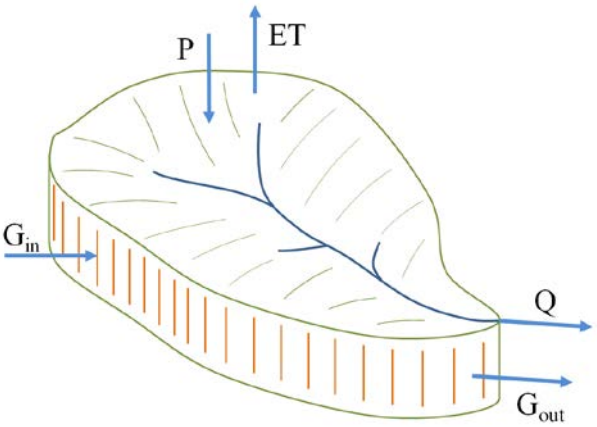

Figure 1. Conceptual model of a catchment, with the components of regional water balance, after Dingman (1994).

When averaged over a long time period, the change of storage can be approximated as zero due to the conservation of volume of water. In addition, ground-water inflow is usually negligible as ground water commonly tends to follow flow paths somewhat similar to the surface flow, that is, towards the pour point. (Dingman, 1994)

2.1.2. Changes in the regional water balance due to urbanization

On urban areas, several mechanisms (e.g. soil sealing) cause the regional water balance to differ from natural conditions (Fletcher et al., 2012). Some alterations in the hydrologic cycle are demonstrated in Figure 2. Most of the water-balance changes related to urbanization are induced by the rising share of impervious surfaces. The effects are further enhanced as even non-sealed surfaces in urban areas often have a practically impervious nature because of compaction.

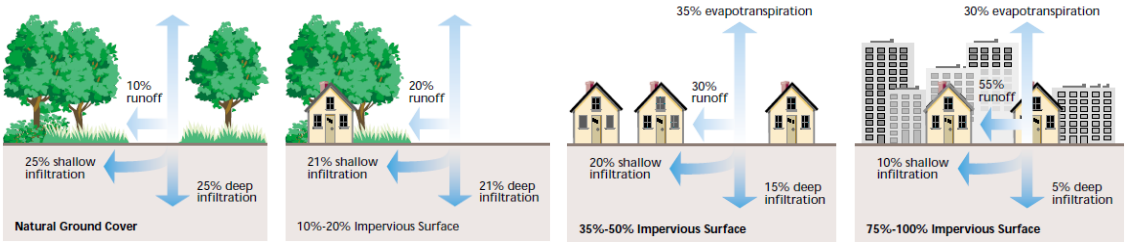

Figure 2. Effects of imperviousness on urban water cycle (Bernard and Tuttle, 1998).

The components of the water balance and the changes in these components due to urbanization shall now be described in more detail.

2.1.3. Precipitation

The origin of precipitation

Like in natural conditions, precipitation is the most important water input mechanism also in the water balance of urban areas. This study mainly focuses on that part of the hydrologic cycle where water is in close contact with land. The process that brings water into this part of the cycle is precipitation. According to Dingman (1994), there are four-steps needed in order for precipitation to occur: (i) The air has to cool down to a temperature close to the dew-point, (ii) condensation nuclei need to be present to form cloud droplets or ice crystals, (iii) these droplets or crystals should grow into raindrops, snowflakes or hailstones, (iv) additional water vapor has to be available for the process to be sustained.

The cooling of air can occur due to several different reasons. However, the most important is the vertical movement of air masses. As unsaturated air rises, it cools down at a dry adiabatic lapse rate of approximately 1 °C per 100 m. At some level, the rising air reaches the dew point and starts to condensate into droplets or ice crystals. The latent heat deliberated slows down the cooling. Therefore, the air cooling starts to follow the moist adiabatic lapse rate or the saturated adiabatic lapse rate, with typical values ranging from 0.5 °C per 100 m to 0.7 °C per 100 m. (Kuusisto, 1986a)

There are three main mechanisms that can cause the upward movement of air. Accordingly, three basic types of precipitation can be named: cyclonic, convective, and orographic. In Finland, the most typical one is the cyclonic precipitation usually generated by chilly polar air flowing from the East colliding with warmer air from the West. At the interface of the two air masses, the warmer air rises over the cold air mass, thus cooling down. Convective precipitation, in turn, is normally triggered by the sun heating the ground surface on a sunny day. On some areas which tend to absorb more heat than their surroundings, the air warms up faster than in the surrounding areas and starts to flow upwards. This may cause heavy but temporally short rain with also potential thunder. The last type of precipitation, orographic, appears when an air mass flows over an area of rising ground level, e.g. a mountain range. Such topography forces the air to rise and thus cool down. Due to geographical reasons this last type does not have a notable effect in Finland, despite small local exceptions. (Kuusisto, 1986a)

As mentioned above, condensation nuclei are needed for the condensation of water to take place. There are usually plenty of these available, originating from forest fires, volcanic activity, meteoric dust, windblown clay minerals, sea salt, etc. Nowadays, in many areas, anthropogenic particles such as nitrogen and sulfur compounds may exist in equal or even larger quantities than the nuclei of natural origin. Dingman (1994)

Due to their small diameter, the fall velocities of cloud droplets are typically rather slow. Thus, the droplets need to grow larger before they can fall down to earth. At above-zero temperatures, it is the random droplet collisions that lead to a gradual growth into raindrops. However, in many cases the temperatures are below the freezing point of water. Pure water can form ice crystals by itself only if the temperature is less than –40 °C. In case of a higher temperature, certain types of icing nuclei are needed to start the ice-crystal growth. Clay minerals work particularly well for this purpose. (Dingman, 1994; Kuusisto, 1986a)

Dingman (1994) shows by example that not even all of the water contained by a thick cloud would produce any substantial precipitation if it was to fall as rain at once. Consequently, it is clear that water vapor needs to be imported into the cloud to enable a proper rainfall take place. The water vapor pressure in a precipitation-producing cloud can be sustained when there are winds converging on the cloud, and thus providing a continuous inflow of water.

Spatial and temporal variability of precipitation

There are several factors affecting precipitation conditions on different regions around the globe. These include latitude, altitude, distance to areas of evaporation, dominating wind directions, position in relation to mountain ranges, and the temperature gradient between sea and continent (Kuusisto, 1986a).

Within Finland, some local spatial variability of precipitation exists. On the coastline, the transition in wind shear stress between sea and land areas may result in upward

airflow and trigger additional rains some 20 km inlands. Another local phenomenon is the orographic effect caused by ridges or hills. Although there are not any mountain ranges in Finland, ridges and eskers of glacial origin do exist. At some locations, they can decrease or increase the seasonal precipitation by as much as 40 % to 80 %, respectively. This is important also from the point of view of this study as the study area is located close to the First Salpausselkä, one of the major ridges in Finland (see Chapter 4.2.3). Last, a third mechanism that can have a local effect on the precipitation is urbanization. The amount of condensation nuclei can be considerably high in the air above urban areas. This, among some other reasons may result in a few percent's rise in the annual precipitation in cities. (Kuusisto, 1986a)

Precipitation varies also with time. It occurs in events with random intervals, intensities, and durations. In addition, there are also seasonal differences, and the intensity of precipitation rarely remains constant even during a single event. Thus, the time-pattern of precipitation typically is highly complex. (Dingman, 1994; Kuusisto, 1986a)

It is typical for the Finnish climate that the rainiest months of the year are July and August. This is due to the heavy convective rainfall which is customary during warm and sunny summer days. However, through most of the year precipitation is largely cyclonic, induced by the relatively warm and moist air masses flowing from the Atlantic. In southern Finland, the average annual precipitation varies from 600 to 750 mm per year. (Kuusisto, 1986a)

Precipitation measurement

Accurate precipitation measurements are crucial for successfully studying and modeling the processes that take place in a catchment. However, these input data always are subject to some degree of uncertainty. This uncertainty is induced by both the methods used for observing precipitation, and the methods used for generalizing the measurements to cover the whole area of the studied system, e.g. the catchment. (Dingman, 1994)

The traditional way of measuring precipitation at a single point is simple. It is done by placing a vessel on an open field and measuring the amount of water caught. The results can be observed at certain intervals, say, once a day, or continuously with an automated metering system. The data gained is typically disturbed by errors from several sources. These include obstructions nearby, losses due to splash, evaporation or wetting, instrument errors, observer errors, errors due to varying observation intervals, and so on. Several different types of precipitation gages have been developed to minimize the impact of different error sources. In addition, the observed values are usually corrected to take into account any known systematic errors. (Dingman, 1994; Kuusisto, 1986a)

Discrete point measurements can be interpolated to obtain the areal precipitation as well as contours describing the spatial variability of precipitation over a region. There are several different mathematical approaches to solve this interpolation (e.g. the one

presented by Thiessen (1911)), but they will not be discussed any further here. At present, an increasing share of precipitation measurements are conducted using radar or satellite observations. The new technology is useful as it can provide very detailed information on the areal precipitation and its spatial variability. Nevertheless, traditional observing still holds its place, as the remote sensing data still needs to be calibrated against ground measurements from rain gages. (Dingman, 1994)

The effect of urbanization on precipitation

On urban areas, precipitation is typically increased compared to natural conditions. This is due to the urban heat island effect and the effect of aerosols such as SO_2 or NO_x in the urban air (Ntelekos et al., 2009). In Finland, these effects are though almost negligible compared to other local factors (Seuna et al., 1986).

2.1.4. Evapotranspiration

Evapotranspiration includes all the processes occurring in the proximity of land or water surfaces that result in evaporation of liquid water into atmospheric water vapor (Dingman, 1994). In the southern parts of Finland, the evapotranspiration sums up to ca. 60 % of the annual precipitation (Vakkilainen, 1986).

Evapotranspiration can be divided into two main components, caused by different physical phenomena. The first one, evaporation, refers to all the evaporation of water from the surface of ground, water, or a snowpack. This takes place when the water molecules on a surface acquire a sufficient amount of energy to escape the surface and enter the gas phase. The energy captured in the process is called latent heat. To be more accurate, both evaporation and condensation usually take place simultaneously. It is the net effect of these two that defines whether evaporation takes place or not. The rate of evaporation is dictated by the difference in partial pressure of water vapor between the air and the surface. (Vakkilainen, 1986)

The other mechanism is transpiration, which means *'the evaporation of water from the vascular system of plants into the atmosphere'* (Dingman, 1994). The plants absorb water from the soil, transport it through the plant body, and evaporate it through small cavities, stomata, located in their leaves. What is remarkable is that the plants can regulate the amount of transpiration through opening or closing guard cells at the openings of stomata. This behavior is influenced by light conditions, humidity, and the amount of water available to the leaves. (Dingman, 1994)

The part of precipitation that gets captured by vegetation before reaching the ground may evaporate straight from these vegetative surfaces. This process is called interception, and the water evaporated is referred to as the interception loss. This loss depends on the type of vegetation, as well as the temporal characteristics and form of precipitation (Dingman, 1994). In urban areas, interception is typically less noteworthy than in rural areas, as urbanization limits the canopy cover to only a reduced portion of the ground area.

One important point of view is the difference between the terms potential evapotranspiration and actual evapotranspiration. The first one refers to the possible evaporation rate if the amount of water in the soil was not limited, and if no advection or heat-storage effects took part. In other words, it assumes evapotranspiration to be energy-limited. In some regions, or during dry seasons, however, the process is limited by the soil water content. Thus, the amount of actual evapotranspiration differs from the potential value. (Dingman, 1994)

The areal actual evapotranspiration can be measured or calculated in a number of ways. These may incorporate water-balance approaches, lysimeter or evaporation pan measurements, as well as empiric or semi-empiric formulas, etc. One of the commonly used methods is the Penman-Monteith equation (Dingman, 1994):

$$ET = \frac{\Delta(K+L)+\rho_a c_a C_{at} e_a^*(1-W_a/100)}{\rho_w \lambda_v[\Delta+\gamma(1+C_{at}/C_{can})]}, \quad (2)$$

where
ET = evapotranspiration rate from a vegetated surface [mm/d],
Δ = slope of the saturation-vapor-pressure vs. temperature curve at the air temperature [mbar/°C],
K = net incoming shortwave radiation [kJ/m^2/d],
L = net incoming long-wave radiation [kJ/m^2/d],
ρ_a = density of air [kg/m^3],
c_a = specific heat of the air [J/kg/°C],
C_{at} = atmospheric conductance for water vapor [mm/d],
e_a^* = saturation vapor pressure at the air temperature [mbar],
W_a = relative humidity [%],
ρ_w = density of water [kg/m^3],
λ_v = latent heat of vaporization [J/kg],
γ = psychrometric constant [mbar/°C],
C_{can} = canopy conductance [mm/d].

Another, more simple empirical method worth mentioning here is the Hargreaves' equation (Hargreaves and Allen, 2003):

$$ET_o = 0.0023 R_a (T_C + 17.8) {T_R}^{0.50}, \quad (3)$$

where
ET_o = evapotranspiration rate [mm/d],
R_a = total incoming extraterrestrial radiation [mm/d],
T_C = temperature [°C],
T_R = daily temperature range [°C].

Alike the Penman-Monteith equation, the Hargreaves' equation is used for calculating the evapotranspiration from meteorological observations data. But, in contrast, the only

input data required by the latter are the air temperatures (Hargreaves and Allen, 2003). This is the method utilized in the SWMM modeling software (see Chapter 2.2.2).

Evapotranspiration on urban areas

There is a documented relation between the degree of soil imperviousness and evapotranspiration. As the imperviousness increases, the rate of evapotranspiration linearly decreases (Haase, 2009). This is mainly due to reduction in vegetation (Fletcher et al., 2012). Thus, the impact of evapotranspiration is somewhat reduced when comparing the urban regional water balance with the rural areas. When considering stormwater modeling of short rainfall events on urban areas, the impact of evapotranspiration may remain almost negligible.

2.1.5. Infiltration

Infiltration is defined as *'the movement of water from the soil surface into the soil'* (Dingman, 1994). It is measured as the infiltration rate – the rate at which water is infiltrating into the soil. The maximum possible infiltration rate of a soil is called the infiltration capacity (or infiltrability). Moreover, the rate at which water arrives to the surface, e.g. through precipitation, is named the water-input rate.

The infiltration process can be limited in one of three different ways. (i) The process can be supply-controlled, meaning the water-input rate is less than or equal to the infiltration capacity, and all the incoming water is immediately infiltrated. (ii) The process may be limited by the infiltration capacity when the capacity is exceeded by the water-input rate. (iii) The rising of the ground-water table to the ground surface level or above may completely stop the infiltration process, setting the infiltration rate to zero. (Dingman, 1994)

Infiltration takes place due to vertical differences in the hydraulic head (Vakkilainen et al., 1986):

$$H = h_g + h_t \,, \tag{4}$$

where
H = hydraulic head [cm],
h_g = elevation head [cm],
h_t = pressure head [cm].

In case the hydraulic head is not constant, its difference over a certain distance is called the hydraulic gradient. The presence of the hydraulic gradient causes water in the soil to flow towards regions of lower hydraulic head. Particularly, if the vertical hydraulic gradient is zero, no vertical flow occurs. In that situation, the water content of the soil column is said to be at the field capacity. If additional water is now brought onto the surface of that soil column, the pressure head, and subsequently, the hydraulic head at

the surface increases. This generates a flow downwards from the surface, and so infiltration occurs. (Vakkilainen et al., 1986; Dingman, 1994):

Infiltration rate at a point rarely remains constant during a single rainfall event. Typically, infiltration rates are high at the beginning of an event. Then they tend to promptly decline, asymptotically approaching a constant value. There are several factors influencing the infiltration rate and its temporal changes:

- the rate at which new water arrives to the surface, or, in case of ponding, the depth of ponds;
- the saturated hydraulic conductivity of the soil profile;
- the initial moisture state of the soil pores;
- soil surface inclination and roughness;
- the chemical characteristics of the soil surface;
- the physical and chemical properties of water. (Dingman, 1994)

Infiltration over an area is hard to determine. This is because infiltration capacity shows great variations even within a range of few meters. In addition, not all the variations can be explained by soil properties, but they are also related to plant and animal activity as well as small-scale topographic features. (Dingman, 1994)

To examine the rate at which infiltration occurs, one must first be familiar with the concepts of hydraulic conductivity as well as the Darcy's Law. The hydraulic conductivity, K_h (cm s^{-1}), describes the relation of the water flow rate through a porous medium with the gradient of potential energy. The main factor affecting the hydraulic conductivity is the size of the cross-sectional area through which water is able to flow. This, in turn, is dictated by the soil-grain size and the degree of saturation. (Dingman, 1994)

The hydraulic conductivity of soil can be measured empirically either in the laboratory or in the field (Vakkilainen et al., 1986). There are, also, plenty of literature values for conductivities of different soil types available for use. Either way, after the hydraulic conductivity is known, the water flow rate in the soil can be determined by applying the Darcy's Law. For vertical unsaturated flow the law is expressed as (Dingman, 1994):

$$q_z = -K_h(\theta)\left[1 + \frac{d\psi(\theta)}{dz}\right], \quad (5)$$

where
q_z = Darcy flux in vertical direction [cm s^{-1}],
$K_h(\theta)$ = hydraulic conductivity [cm s^{-1}] as a function of soil-water content θ,
$\psi(\theta)$ = pressure head [cm] as a function of soil-water content θ,
z = elevation [cm].

As can be noted from Equation 5, the hydraulic conductivity and the pressure head are both functions of soil-water content. These relations need to be properly known in order to get a good estimate for the vertical Darcy flux. When trying to make such an estimate, however, one faces the challenge that the water contents, gradients and conductivities change over both place and time. (Dingman, 1994)

A common physically-based theoretical approach for calculating infiltration is the Richards Equation. It is derived from the Darcy's Law and the principle of conservation of mass. Nevertheless, its non-linear nature allows for only numerical solutions. Hence, the solution can be approximated e.g. by the Philip's Equation, of which typically only the two first terms are considered (Dingman, 1994):

$$f(t) = \frac{S_p}{2} t^{-\frac{1}{2}} + K_p \,, \tag{6}$$

where
$f(t)$ = infiltration rate [cm s^{-1}],
S_p = sorptivity [cm $s^{-1/2}$],
t = time [s],
K_p = hydraulic conductivity [cm s^{-1}].

However, the Philip's Equation has some limitations. It lacks parameters for the characteristics of the rainfall or snowmelt, for example. (Dingman, 1994)

The Green-and-Ampt Model (Green and Ampt, 1911), based on the same principles as the Richards Equation but formulated differently, provides a '*more holistic and informative view of the infiltration process'* (Dingman, 1994). It is able to nicely present the complete infiltration until surface ponding takes place, as well as the decline of the infiltration capacity thereafter. In addition, the soil parameters needed are easily measurable physical properties. Hence, it is one of the most widely used approaches for modeling the infiltration process, and several other models and extensions have been built on it (Dingman, 1994). The Green-and-Ampt Equation for infiltration capacity as a function of time is formulated as:

$$f(t) = K_h^* \left[1 + \frac{|\psi_f|(\phi - \theta_0)}{F(t)}\right], \quad t_p \le t \le t_w \,, \tag{7}$$

where
$f(t)$ = infiltration rate [cm s^{-1}],
K_h^* = hydraulic conductivity [cm s^{-1}],
ψ_f = effective tension at the wetting front [cm],
$(\phi - \theta_0)$ = initial soil water deficit [-],
$F(t)$ = cumulative depth of the wetting front [cm],
t_p = time of ponding, or the instant of the surface layer becoming saturated [s],
t_w = instant of the entire soil column becoming saturated [s].

The underlying assumptions of the Green-and-Ampt Model include the vertical soil water-content profile to be initially homogeneous, and the wetting front to be considered as a distinct discontinuity in that profile. The results of the model have been found to substantially correspond with the numerical results of the Richards Equation. (Dingman, 1994)

As stated above, infiltration capacity can vary greatly even over short distances. According to Kabat et al. (1997), using sufficiently detailed soil data as an input for areal modeling would in most cases result in too large an effort. This could be somewhat resolved by averaging these data over a larger area, thus compromising over the spatial resolution. Furthermore, they proposed the best results could be obtained by treating the soil infiltration capacity parameters as calibration parameters instead of exact physical properties of the soil.

Another process that should be at least briefly mentioned when considering the infiltration in Finland is the formation of frost in the soil. When the temperature in the soil pores drops below 0 °C the soil water starts to freeze. As a result, a capillary flow of additional water towards the freezing front takes place via the liquid water layer on the surfaces of the soil grains. This additional water is imported until most of the water in the pores has frozen. However, this phenomenon is not being further discussed here. Nevertheless, it should be remarked that less to none infiltration occurs when the soil is frozen. (Vakkilainen et al., 1986)

Infiltration reduction caused by impervious surfaces

In urban areas, impervious surfaces eliminate infiltration and thus increase surface runoff (Fletcher et al., 2012). Reduced infiltration also affects groundwater recharge and results in lowered groundwater levels. The effect may be enhanced through groundwater seepage into drainage networks. Lowered groundwater levels may for example pose problems for groundwater use and reduce the base flows of urban streams.

2.1.6. Snow and snowmelt

In Finland, a considerable share of the annual precipitation falls in the form of snow. The fraction is approximately 30 to 40 % for the south of Finland (Kuusisto, 1986a). Snow is a porous medium consisting of ice as well as pores filled with air or liquid water (Dingman, 1994). The density of new-fallen snow is typically ca. 100 kg m^{-3}, but can, in cold conditions, remain even several times smaller (Kuusisto, 1986b).

This chapter discusses the processes related to snow and snowmelt. But, before going into more detail, some concepts important for understanding the properties of snow are presented in Table 1 below.

Table 1. Snow parameter definitions and methods of measurement (Dingman, 1994).

Parameter	Definition	Measurement
Precipitation	The depth of the water equivalent of all forms of precipitation during a time period	Melting or weighing standard gages; Universal gages; Radar observations
Snowfall	The incremental depth of new-fallen snow (or other solid precipitation) during a time period	Rulers and boards laid down before a snowfall event; Universal gages; Radar observations
Snowpack	The depth of snow accumulated on the ground at a certain moment	Snow stakes (rods fixed to the ground, with elevation markings on them); Snow surveys at fixed snow courses (snow tube measurements at several points in a line); Snow pillows that weigh the snow; Acoustic gages; Radioactive gages; Microwave, radar, and satellite observations
Snowmelt	The depth of liquid water from melting that leaves the snowpack during a time period	Lysimeters (measuring the water draining from the snowpack); Snow pillows; Universal gages
Ablation	The depth of loss of water from the snowpack through snowmelt, evaporation and sublimation during a time period	Lysimeters (measuring the water draining from the snowpack); Snow pillows; Universal gages; Pans that are accurately weighed
Water output	The depth of liquid water from rain and snowmelt that leaves the snowpack during a time period	Lysimeters (measuring the water draining from the snowpack); Snow pillows; Universal gages

The period when the snow water equivalent has an increasing trend is called the accumulation period. When there is a layer of snow on the ground, a process called metamorphism takes place within the snow. This process is driven by four different mechanisms: (i) gravitational settling, (ii) destructive metamorphism, (iii) constructive metamorphism, and (iv) melt metamorphism (Dingman, 1994). In sum, these induce the continuous increase of the snowpack density until it reaches values of 330 to 350 kg m^{-3} (Kuusisto, 1986b). During snowmelt period, the capacity of snow to retain liquid water starts to decrease and increasing amounts of runoff are generated up until the snow has completely melted.

What makes snow different from other forms of precipitation is the delay between the snowfall event and the creation of runoff. Snow can store the water for extended periods, say, months, before the normal processes of the land phase of the hydrological cycle follow. However, at some point the seasonal snow always enters the melt period. This period can be divided into three phases. (i) The warming phase, during which the average temperature of the snowpack gradually increases all the way up to the melting point. No melting yet occurs, though. (ii) The ripening phase, through which melting already takes place but the meltwater still is retained within the snowpack. (iii) The output phase, when all additional energy inputs directly result in water output. Nonetheless, it should be acknowledged that practically these phases somewhat mix up due to air temperature fluctuations on both sides of the melting point, for example. (Dingman, 1994)

Maybe the most important parameter considering the hydrological effects of snowmelt is the rate of water output from the snowpack. Water, also in its liquid phase, can be retained within the snowpack, and thus the rate of water output is hydrologically even more noteworthy than the actual rate of melting of the snow. In Finland, the extreme for water output of a snowpack may even reach values of 20 to 30 mm d^{-1} on open grounds. On forested areas, the values are typically 30 to 60 % smaller. (Kuusisto, 1986b)

Snowmelt is largely controlled by the energy balance of the snowpack defined by the following equation (Kuusisto, 1986b):

$$H_m = H_{sn} + H_{ln} + H_c + H_e + H_p + H_g - H_t \,, \tag{8}$$

where
H_m = heat available for melting [W/m^2],
H_{sn} = net shortwave radiation [W/m^2],
H_{ln} = net long wave radiation [W/m^2],
H_c = sensible heat exchange [W/m^2],
H_e = latent heat exchange [W/m^2],
H_p = advective heat of precipitation [W/m^2],
H_g = heat transfer at the lower surface of the snowpack [W/m^2],
H_t = change in the heat storage of the snowpack [W/m^2].

Under most conditions, the impact of the radiation balance is dominant. The sensible heat exchange may have a large effect, too, especially on windy, rainy days. Owing to the first mentioned, the albedo of the snowpack greatly influences the rate of melting. New-fallen snow has an albedo of ca. 80 %, and the value decreases during the melting season until 40 to 50 %, unless new snow falls again. (Kuusisto, 1986b)

When studying the snow properties for areas instead of points, the local variations of topography (e.g. aspect) and land cover (e.g. canopy) are of major importance. These factors may affect the amount of energy-input from solar radiation, the canopy interception of snow, and the wind conditions, just to name a few. This poses some challenges for correctly measuring the areal values of snow accumulation and snowmelt. (Dingman, 1994)

Snowmelt is typically being modeled using two different types of models. On the one hand, there are the physical-based models that build on the energy balance of the snowpack. On the other hand, melting can be modeled with the simple and partly empirical temperature-index approach. In addition, there are hybrid models trying to exploit the best parts from both of the above. The energy-balance based approach craves for meteorological observations more detailed than needed for the temperature-index approach. Relatedly, the first mentioned has proven accurate for point snowmelt modeling. However, it is not manageable to implement it on larger areas because of the above mentioned extensive local variations of several parameters, and the lack of data

concerning these. Thus, temperature-index and hybrid approaches are better suitable for catchment-scale modeling. (Dingman, 1994; Kuusisto, 1986b)

The temperature-index approach draws a linear correlation between the average air temperature and snowmelt (Dingman, 1994):

$$\Delta w = M(T_a - T_m)\,, \qquad T_a \geq T_m; \tag{9}$$
$$\Delta w = 0\,, \qquad T_a < T_m.$$

where
Δw = snowmelt [mm d^{-1}],
M = degree-day factor [mm °C d^{-1}],
T_a = average air temperature [°C],
T_m = threshold temperature for melting [°C].

Here, the degree-day factor (also known as the melt coefficient) varies with different conditions. In Finland, it ranges from 3.5 mm °C d^{-1} on open grounds to less than 1.2 mm °C d^{-1} for a thick forest. On a catchment-scale the typical values fall between 2.0 to 3.0 mm °C d^{-1}. (Kuusisto, 1986b)

2.1.7. Surface and subsurface event flow

Surface runoff is a process that takes place on saturated sloping surfaces. As mentioned above in Chapter 2.1.4, input of water to a saturated surface causes ponding. If the depth of ponding (d) grows higher than the roughness of the ground (d_p), and the ability of surface tension to hold water motionless becomes exceeded, overland flow occurs (see Figure 3). (Dingman, 1994)

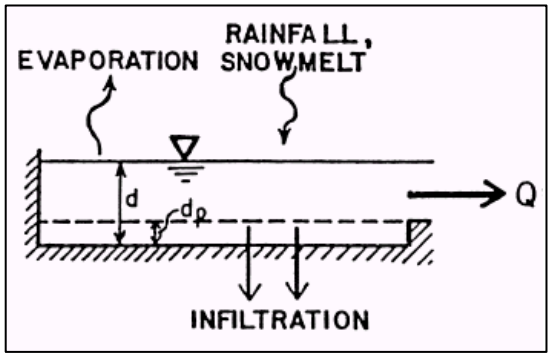

Figure 3. Conceptual view of surface runoff in SWMM, from Rossman (2010).

Two main mechanisms can cause the saturation of a surface. First, it can be saturated from above (Horton, 1933). The resulting phenomenon is called Hortonian overland flow. It is considerable especially during intense rainfalls preceded by dry catchment conditions, or areas where the conductivity of the soil surface is low, the latter including e.g. urban impermeable areas as well as areas with soil frost. Second, saturation from below may result in saturation overland flow (Dunne, 1978). In that case, the ground-water table rises up to the level of the ground surface, constraining all additional water input to become overland flow.

Overland flow is not the only process leading to stream response after rainfall events. In some soils, subsurface event flow can be of importance, too. Typically, this flow takes place in soil layers just below the surface and not connected to the regional ground-water aquifer. Depending on the circumstances, the subsurface event flow may form – and flow through – either a saturated or an unsaturated zone in the soil. Especially hillslopes containing macropores can produce rapid subsurface responses, as the macropores enable the water to bypass the soil matrix of lower hydraulic conductivity. One classic situation is called the sloping slab, which occurs on hillslopes with a thin layer of permeable soil on top of a less permeable layer, say, clay. In such a case, subsurface flow is likely to happen through the upper layer. (Dingman, 1994)

During a rainfall event with a constant intensity, the overland flow keeps growing over time. Theoretically, the growth continues until the surface of the whole catchment is saturated. Due to irregularities in the small-scale surface topography, the surface runoff tends to form small streams already within minutes (Hyvärinen and Puupponen (1986). In the subsurface layer, the channelization may take some hours. Gradually, these low-order streams merge and form repeatedly higher-order streams. The properties of the channelized flow are being discussed further in the next chapter.

Not all of the precipitation results in formation of runoff. The term effective precipitation refers to the part of the rainfall that creates runoff immediately or shortly after the rainfall event. Thus, it excludes the part that is evapotranspirated or captured into the ground-water storage, for example. Hence, effective precipitation results in a corresponding amount of direct runoff from the area. (Dingman, 1994)

2.1.8. Channel flow and pipe flow

As noted above, the overland flow channelizes rather easily. These channels may appear in all kinds of depressions, including gutters, ditches, etc. On urban and sub-urban areas, some or all of the flow is usually collected into underground stormwater or combined sewer network. To understand these conduit systems, one should be familiar with the basics of open-channel flow as well as closed-conduit flow. There is a wide variety of flow routing methods for modeling these flows. Some of these are briefly discussed below.

Open-channel flow

Despite of its name, open-channel not only takes place in ditches and streams, but also sewers not flowing full. This includes most stormwater conduits, as they are typically designed to operate well below their full depth, mainly to avoid flooding.

The nature of open-channel flow is in most real cases highly complex. Therefore, before modeling it, some assumptions are usually made (see e.g. (Durrans, 2003)). These include one-dimensional flow, hydrostatic pressure distribution, constant water density, and channel length much greater than the flow depth. The Saint-Venant equations, based on mass continuity and the conservation of momentum, are partial differential

equations accurately describing flow in these conditions. These equations can be written in several forms, but cannot be solved analytically, only numerically. The numerical solution of the complete Saint-Venant equations is called the dynamic wave routing. It may be done with the finite difference or the finite element method, for example. The 1-dimensional Saint-Venant momentum equation can be arranged as follows:

$$Q = Q_N(1 - \frac{1}{S_x}\frac{\partial y}{\partial x} - \frac{u}{S_0 g}\frac{\partial u}{\partial x} - \frac{1}{S_0 g}\frac{\partial u}{\partial t})^{1/2} , \quad (10)$$

where
Q = actual unsteady flow [m^3/s],
Q_N = flow under normal conditions [m^3/s],
S_0 = slope of the channel bed in longitudinal direction [-],
u = flow velocity in the longitudinal direction [m/s]. (Durrans, 2003)

Various approximations of the Saint-Venant equations have been developed, e.g. kinematic, diffusion, and gravity waves. For instance, when flow changes are slow and the depth-discharge relationship is not considerably looped the two last terms in the parentheses in Equation 10 can be ignored. This yields the kinematic wave approximation:

$$\frac{\partial Q}{\partial t} + c\frac{\partial Q}{\partial x} = 0 , \quad (11)$$

where
c = kinematic wave celerity, dQ/dA [m/s]. (Durrans, 2003)

In some applications, even the steady-flow routing can be sufficient. It directly translates and sums the inflow hydrographs to acquire an outflow hydrograph. The relation between discharge and flow depth can then be solved using e.g. the Manning equation (Durrans, 2003):

$$V = \frac{C_f}{n} R^{2/3} S_0^{1/2} , \quad (12)$$

where
V = flow velocity [m/s],
C_f = unit conversion factor [$m^{1/3}/s$]
n = friction factor [-],
R = hydraulic radius [m],
S_0 = channel slope [m/m].

The friction factor *n* in Equation 12 is often referred to as the 'Manning's roughness coefficient *n*'. It is largely defined by the surface material of the streambed or the pipe, and plenty of *n* values for different materials appear in the literature.

In stormwater modeling, it is also important to understand overland flow. Overland flow refers to thin sheet-flow that occurs before the runoff gets channelized due to surface

irregularities. The length of true overland flow is rarely more than 100 m. The open-channel flow routing principles can typically be applied to overland flow as well. Overland flow modeling may however need huge simplifications as the irregularities of the land surface are typically substantial compared to the thickness of the overland flow layer. The Manning equation may be used for turbulent overland flow, yet keeping in mind that the roughness coefficient *n* may vary considerably depending on the Reynolds number. (Woolhiser, 1981)

Closed-conduit flow

As opposed to open-channel flow, closed-conduit flow occurs in pipes that are full with water, i.e. there is no free water surface in the cross-section of the pipe.

The pipe flow is typically modeled based on conservation of energy. According to the energy equation the sum of pressure, elevation, and velocity heads must equal between two cross-sections of a pipe, excluding energy losses and inputs on the way. Thus, evaluating the losses is a central part of the modeling. These losses can be classified into either frictional or local losses, of which the first mentioned are, in most cases, of higher significance. (Durrans, 2003)

The energy loss due to friction can be solved e.g. from the Darcy-Weisbach equation:

$$h_L = f \frac{L}{D} \frac{V^2}{2g}, \tag{13}$$

where
h_L = head loss due to friction [m],
f = friction factor [-],
L = pipe length [m],
D = pipe diameter [m],
V = cross-sectional averaged flow velocity [m/s],
g = acceleration of gravity [9.81 m/s^2].

Several other methods of computing the frictional loss exist, too, including the Manning equation (Eq. 12), the Chézy equation, and the Hazen-Williams equation. (Durrans, 2003)

2.2. Rainfall-runoff modeling

2.2.1. What is rainfall-runoff modeling?

Modeling can be defined as simulating the natural world with a model representing a part of that world. Mathematical models are *'explicit sets of equations and numerical and logical steps'*, converting numerical inputs to numerical outputs (Dingman, 1994). According to e.g. Karvonen and Kettunen (1986) and Dingman (1994), conceptual modeling consists of the following steps:

- conceptualization of the problem;
- selection (or development) of a suitable model;
- parameter sensitivity analysis *a priori*;
- model structure identification and parameter estimation (or calibration);
- model verification;
- model acceptance testing (or validation);
- parameter sensitivity analysis *a posteriori*.

Rainfall-runoff modeling predicts the hydrological response (runoff) to a certain input (precipitation), usually as a function of time. The mechanisms of prediction differ. So-called 'black-box models' (or the systems view) seek for an abstract function relating the input and output functions, whereas physically-based models try to thoroughly describe the underlying processes. In practice, most rainfall-runoff models fall between these two extremes. (Dingman, 1994)

When applying the systems approach, the systems modeled can be classified into two categories: (i) linear and (ii) non-linear. A system is linear if for input au_1+bu_2 applies (Karvonen and Kettunen, 1986)

$$z(t) = f(au_1 + bu_2) = af(u_1) + bf(u_2) = az_1 + bz_2 \,, \qquad (14)$$

where
$z(t)$ = model output;
$x(t)$ = state of the model;
$u(t)$ = model input;
$f(x(t), u(t), t)$ = arbitrary function;
a, b = any two scalar quantities.

Spatial boundaries of the system are typically defined according to catchment borders. Conceptually, the modeled system can either include all the hydrological processes in a catchment system, or be restricted to a surface runoff system. The difference is that the surface-runoff system uses only the fraction of precipitation that actually causes runoff as input, known as the effective precipitation. Another difference is that the catchment system, due to its complexity, is evidently non-linear. In contrast, the surface-runoff system can at times be reasonably approximated as being linear. (Diskin, 1981)

The rational method is a typical example of a linear surface-runoff model:

$$q_{pk} = C_R i_{eff} A_D \,, \tag{15}$$

where
q_{pk} = peak discharge [m3 s^{-1}],
C_R = runoff coefficient [-],
i_{eff} = rainfall intensity [mm h^{-1}],
A_D = catchment area [km^2]. (Dingman, 1994)

The rational method assumes a simple linear correlation between the effective rainfall intensity and the peak discharge induced. Thus, this method is typically used for calculating the peak flows induced by a rainfall with a certain intensity or return period, and is widely used in design purposes in urban areas. The runoff coefficient used as a parameter is catchment-specific, varying with land use and other catchment properties. The values for the coefficient are highest for impermeable surfaces such as pavements and rooftops. (Dingman, 1994)

Due to its simplicity, the rational method has some major limitations. It works well only in small catchments with areas less than 80 hectares. Also, the method cannot account for any larger storage such as detention ponds in the catchment area. (Texas Department of Transportation, 2011)

As stated above, physically-based models describe physical processes occurring in the catchment area, including precipitation, evapotranspiration, infiltration, snowmelt, overland flow, channel flow, and ground-water flow. Some common methods for modeling these processes were presented in Chapter 2.1. Next, a computer software for combining these is introduced.

2.2.2. The EPA Storm Water Management Model (SWMM)

There are numerous different rainfall-runoff simulation software packages for all kinds of modeling purposes (Zoppou, 2001). The EPA Storm Water Management Model (SWMM) is one of the most commonly used. Among all similar software, this study focuses on SWMM for a few reasons. (i) SWMM is widely used in analysis and design of stormwater drainage systems, especially on urban areas. (ii) There have been previous studies carried out on the same geographical area using the same software. (iii) The U.S. Environmental Protection Agency (EPA) provides the SWMM model and a related graphical user interface free of charge.

SWMM was first developed in 1971, and has since then been upgraded several times. The current version (number 5) was completely re-written by the U.S. EPA and a consulting firm of CDM, Inc. (Rossman, 2010)

SWMM can be used for a range of applications. It is suitable for modeling either single precipitation events or continuous modeling of multiple events. The simulation period

consists of multiple time steps, and SWMM can track both runoff quantity and quality for each time step. The model is conceptually divided into four major environmental compartments: (i) the atmosphere compartment, accounting for precipitation and pollutants from air; (ii) the land surface compartment, modeling areas receiving precipitation and generating runoff; (iii) the transport compartment, routing flow from runoff source areas through a network of pipes, channels, etc.; and (iv) the ground-water compartment, receiving infiltration from the land surface and providing input to the transport compartment. Of these, (ii) and (iii) are discussed in more detail below. The objects and processes in these four compartments account for all the major components affecting the regional water balance (see Chapter 2.1.1). (Rossman, 2010)

The land surface compartment

The processes occurring on the land surface are an essential part of SWMM. For modeling, the land surface is commonly divided into small, sufficiently homogeneous subcatchments, each draining to a single discharge point. All of the subcatchments have their own sets of hydrological parameters such as imperviousness and depression storage. Based on these, several hydrological phenomena are simulated during every time step. (Rossman, 2010)

Water input to the subcatchments is deducted from the atmosphere compartment. Each subcatchment is assigned a Rain Gage element, containing data on rainfall intensity or volume at certain time intervals. (Rossman, 2010)

If there is standing water on subcatchment surfaces, evaporation occurs. Evaporation rates (e.g. daily or monthly) can be defined by the user, or they can be computed from a data series of daily air temperatures. In case they are computed, the Hargreaves' method (see Equation 3) is used. In addition to daily air temperatures, the site's latitude must be known. (Rossman, 2010)

SWMM offers a selection of three different built-in infiltration models. These are (i) the Horton's equation (Horton, 1933), (ii) the Green-and-Ampt method (Green and Ampt, 1911), and (iii) the Curve Number method. Infiltration only takes place on the pervious fraction of the subcatchment, defined by the imperviousness parameter. To model the ground-water conditions more precisely, one can include optional Aquifer objects in the model. Aquifers simulate the vertical movements of ground water and may exchange water with the drainage system, e.g. through leaking pipes. (Rossman, 2010)

In cold conditions, precipitation may be stored in an assigned Snow Pack object. These objects have parameters for modeling snow accumulation and snowmelt within the subcatchment. In addition, snow removal can be accounted for using a special set of parameters. (Rossman, 2010)

Both precipitation and snowmelt can import water on the subcatchment surfaces. SWMM conceptualizes the creation of surface runoff based on the same principles as presented in Chapter 2.1.6. (Rossman, 2010)

SWMM calculates the outflow from a subcatchment as follows (Park et al., 2008):

$$Q = \frac{W}{n}(d - d_p)^{5/3} S_0{}^{1/2} , \qquad (16)$$

where
Q = subcatchment outflow [m^3/s],
W = subcatchment width [m],
n = Manning's roughness coefficient [-],
d = water depth [m],
d_p = depth of depression (retention) [m],
S = slope [%].

Surface runoff generated at the source areas is defined to flow either into another subcatchment or into a drainage system entry point. (Rossman, 2010)

The transport compartment

The other major part of SWMM is the transport compartment. It describes the hydraulic routing of runoff and possible external inflows through a network of pipes and channels, also known as conduits. These conduits are the links of the drainage network, joined together at junction nodes, which can represent manholes, pipe connection fittings, etc. Typical conduit parameters include invert elevations at both ends, the conduit length, the Manning's roughness coefficient *n*, and cross-sectional geometry. Similarly, junction nodes have parameters such as invert elevation and depth from the ground surface. There are also other possible types of nodes, e.g. flow dividers, storage units, pumps, and flow regulators. (Rossman, 2010)

SWMM offers three different options of flow routing: (i) steady flow routing, (ii) kinematic wave routing, and (iii) dynamic wave routing. These methods were briefly presented in Chapter 2.1.7. The choice of the routing method affects the accuracy of the results, as well as the time taken by running a simulation. (Rossman, 2010)

Flows exceeding the capacity of the drainage system may cause ponding. This means temporarily storing the excess volume at a certain junction, and allowing this pond to dry when system capacity is again available. Ponding can also be disabled by the user, causing all excess volume to overflow the system and be lost. (Rossman, 2010)

Calibration against data

SWMM parameters should typically be calibrated and validated against measurements to reach reliable results. However, some of the model parameters are quite straightforward to deduct from e.g. accurate spatial data and can be reasonably defined even without calibration. Those include subcatchment areas and slopes, for instance. On the other hand, parameters such as the flow width, the depression storage, the roughness coefficients, and the infiltration parameters involve larger uncertainties and are commonly used as calibration parameters. Nevertheless, also the first mentioned

‘straightforward’ parameters involve uncertainties and are often calibrated for a better fit. (Liong et al., 1991)

2.3. Previous studies

2.3.1. The effect of spatial resolution on rainfall-runoff modeling

This study mainly concentrates on the parameterization of a SWMM rainfall-runoff application. The first step in such a parameterization is the catchment delineation and subdivision. Chen and Tucker (2003) compared different approaches for catchment delineation, e.g. to burn a stream network into a digital elevation model (DEM) and to use the *Watershed* tool in ArcGIS (Esri, 2012). They concluded that GIS is a powerful tool for catchment delineation if there are comprehensive and accurate spatial data sources available and the details of the sewer system are correctly accounted for. They also add that manual fine-tuning is often necessary after the automated delineation process.

Based on the spatial resolution, GIS-based catchment modeling can be divided into distributed (or high-resolution) and aggregated (or low-resolution) approaches. A distributed model accounts for all minor spatial variations within the study area while an aggregated model excludes and generalizes details of the input data. Highly distributed models are typically used e.g. for modeling event peak-flows, whereas the more aggregated approaches are mainly suitable for studying large-scale processes like climate change as their limitations are less relevant in long-time-scale modeling. The difference between these two is the level at which features within the catchments are aggregated, i.e. the size of the subcatchments modeled. Aggregation results in loss of complexity but, simultaneously, makes data collection easier. Even the most distributed models usually incorporate some aggregated parameters due to the lack of fully-detailed data on spatial variations of parameters. The key question remains, which level of aggregation is still acceptable in order to maintain a certain degree of accuracy in modeling. (Jacobson, 2011)

Park et al. (2008) performed SWMM simulations with varying levels of subcatchment aggregation. They concluded that the simulated surface runoff was not affected by the spatial resolution of the model. On the other hand, accumulated pollution loads were reduced with an increasing level of aggregation. The peak flows appeared at slightly different time instants but otherwise the hydrograph was not affected by the model aggregation. Similarly, Ghosh and Hellweger (2011) did SWMM runs for 50 storm events. Their results indicated that the annual runoff is not dependent on the spatial resolution of the model. The effect of spatial resolution on simulated peak flows was altered. While for small storms the peak flows increased with an increasing level of aggregation a decrease was found for large storms.

On the contrary, Smith et al. (2005) found that the aggregation level of the catchment affected the difference between measured and simulated runoff volumes. They

recommended minimizing those differences through calibration of model parameters such as the flow width.

For natural catchments, Jang et al. (2007) found out that non-calibrated SWMM models were most accurate if the whole catchment was modeled as one single runoff unit. Those models provided good simulation results without calibration for three undeveloped Korean watersheds with areas ranging from 8.5 km^2 to 55.9 km^2.

There have also been several studies regarding the aggregation level of other rainfall-runoff models similar to SWMM. Thompson and Cleveland (2009) concluded that fully-distributed modeling with HEC-HMS is not feasible in cases where no calibration data is available. The possibilities of scaling the input data of the distributed KINEROS model to match different aggregation levels were studied by Thieken et al. (1999). The outcome was that the flow length could be used as a scaling factor for adapting the same model to catchment delineations of different scales. Zhang et al. (2013) summarized several previous studies and concluded that the flood volume is insensitive to the degree of catchment subdivision. They also noted that only a few studies have concentrated on the effect of catchment subdivision on water balance components like evapotranspiration and infiltration. Their results with a HEC-HMS model showed that (i) overland flow length increases with increasing subcatchment area, (ii) infiltration parameters are independent of the model aggregation level, (iii) the quality of results decreases if the number of subcatchments is too large or too small, and (iv) unlike in previous studies, the aggregation level affects the components of the water balance. Zhang et al. (2013) also conclude that catchment subdivision is useful if detailed data on parameter variations between the subcatchments is available.

Besides the surface runoff processes, also the conveyance system is subject to generalization. The sewer network may be ‘skeletonized’ by disregarding minor pipes. The combined sewer modeling protocol of Department of Water Management for the City of Chicago defines, for example, that no conduits with a diameter smaller than 1070 mm are modeled, unless they have substantial hydraulic importance in the sewer system (Cantone and Schmidt, 2013). This results in only one tenth of the conduits being modeled.

2.3.2. Estimating and calibrating SWMM parameters

A SWMM application includes numerous different parameters, of which several vary from subcatchment to subcatchment. These parameters can be classified to measured parameters (e.g. subcatchment area; pipe lengths, pipe shapes, bed slopes, and diameters; manhole type; soil types; land-use types; and rainfall depth) and inferred parameters (e.g. flow width; infiltration parameters; Manning’s *n* for pervious and impervious areas; depression storage for pervious and impervious areas; imperviousness; and Manning’s *n* for conduits) (Choi and Ball, 2002). The measured parameters are typically easier to obtain, while the inferred parameters usually need to

be calibrated. Nevertheless, also the first mentioned may sometimes involve large uncertainties arising from e.g. inaccuracies in subcatchment delineation.

However, if no runoff measurements required for calibration exist, literature values can be found for several of these parameters. Many parameter values are suggested e.g. in the SWMM User's Manual (Rossman, 2010). In contrast, other parameters such as flow width, hydrological slope, and imperviousness have to be obtained from spatial data. Methods of acquiring values for these parameters without calibration are further discussed in Chapter 5.2.

Detailed spatial data on land cover types etc. is important for calibrating SWMM applications for urban catchments (Jacobson, 2011). Because such data is not always available, there have been attempts to reduce the complexity of the calibration process by concentrating only on the parameters the model is most sensitive to. The problem is, however, that SWMM is sensitive to different parameters in different catchments (e.g. Beling et al., 2011). This highlights the importance of always performing a sensitivity analysis before model calibration. In addition, the method of sensitivity analysis affects the obtained model sensitivity to different parameters (Jacobson, 2011).

Whether calibration could be left undone in some cases is an interesting question. According to Jang et al. (2007), even a non-calibrated SWMM model performs better than an ordinary hydrograph when modeling urbanizing (or urbanized) areas. Amaguchi et al. (2012) developed a vector-based distributed model similar to SWMM which was able to achieve a good reproduction of observed stream flows. However, they recognized the demand of detailed spatial data, and recommended calibration of some parameters (e.g. imperviousness) if only possible.

Overall, it seems there have been experiments with calibrated SWMM models of a low spatial resolution, as well as with non-calibrated high-resolution SWMM models. No studies were yet found where a low-resolution model was applied without calibration to a large urban area for continuous simulation. Thus, the application of this approach is definitely both interesting and challenging.

3. METHODOLOGY

Figure 4 presents the methodology of this work as a flowchart. The numbers indicated in the flowchart refer to corresponding text chapters. The work is based on a variety of spatial data and weather observations which are utilized through GIS analyses and subsequent stormwater modeling. GIS is applied in order to (i) select appropriate study sites, (ii) delineate and subdivide study catchments, and (iii) parameterize the study subcatchments and related stormwater systems for use in stormwater modeling. Using these parameterizations, SWMM simulations are conducted and their results analyzed to assess the suitability of the methods used.

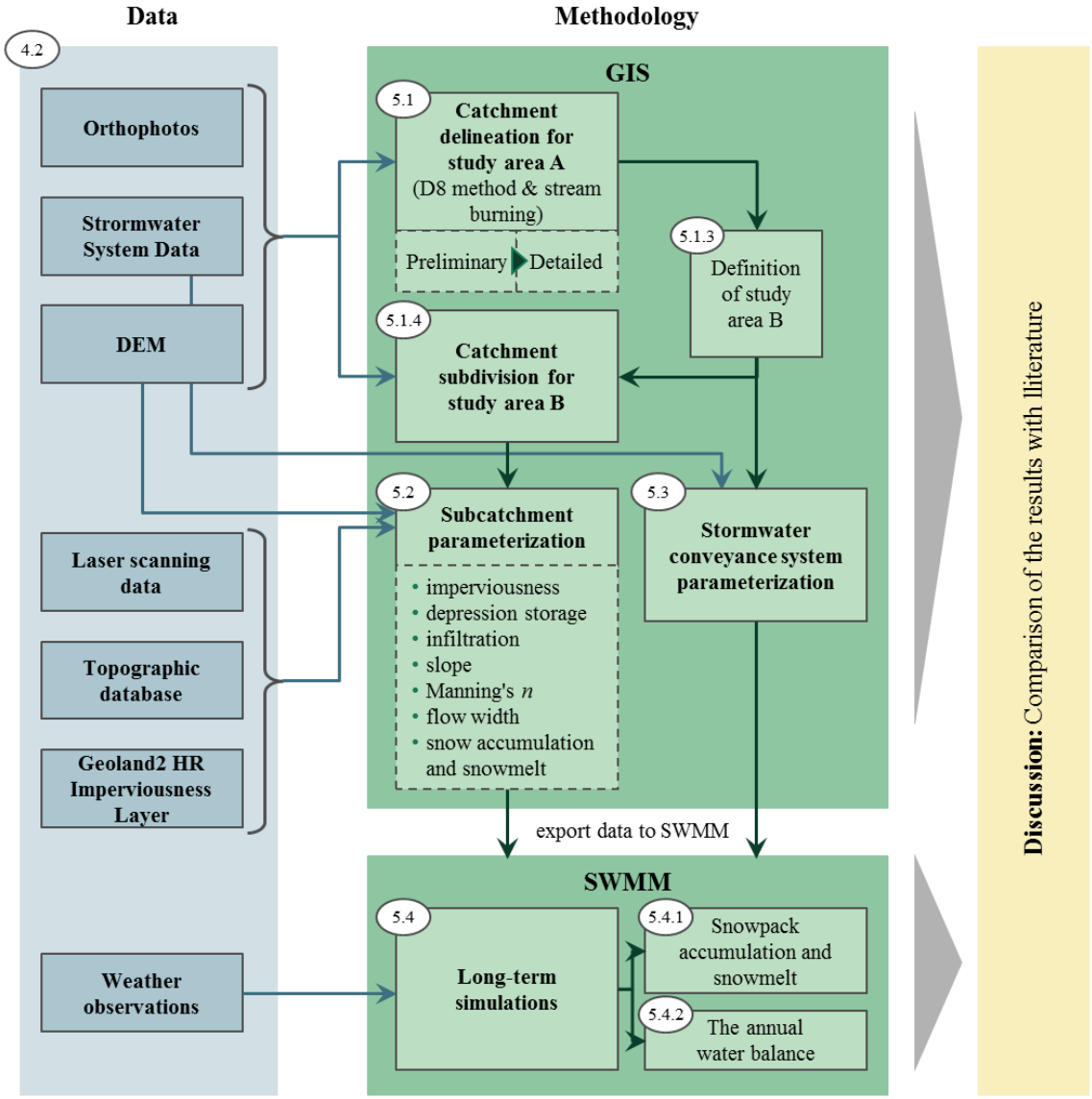

Figure 4. A flowchart of the methodology of the study, with numbers referring to relevant text chapters.

4. STUDY SITE AND DATA

4.1. Study site

The study area lies in the city of Lahti, in southern Finland (see Figure 5). Coarse catchment delineation was performed for an area of 40 km^2 ('study area A') covering ca. 30 % of the lands of Lahti municipality. More detailed studies were conducted for two urban catchments with net area of 2.64 km^2 ('study area B' in Figure 5).

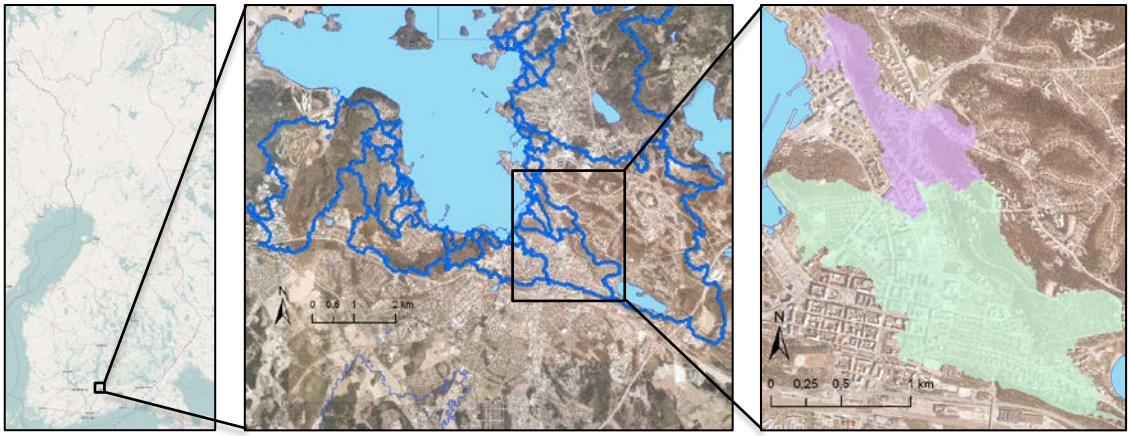

Figure 5. Location of areas studied. The blue lines in the middle indicate the catchment borders of the study area A. The study area B (on the right) covers a fraction of the area A. See Chapter 4.1 for details on how the geographical scope was defined.

The study area B covers parts of the center of Lahti, as well as some residential areas around the city center. Some forested areas of mainly pine woods and mixed forest are also included.

Some hydrological conditions of the study area are presented in Table 2 below. Local hydrology is largely affected by the glacial ridge right next to the study area. Also the geological and topographic conditions in the study area are dictated by glacial formations. More discussion on these will follow in Chapter 4.2.3.

Table 2. Hydrologic conditions in the city of Lahti. The figures are from Laune weather station; see Chapter 4.2.3 for further discussion. (Kersalo and Pirinen, 2009)

Parameter		Value	Time / time period
Annual precipitation	Min.	435 mm	1976
	Mean	633 mm	1971 - 2000
	Max.	896 mm	2008
Monthly precipitation	Min.	2.3 mm	February 1994
	Max.	193 mm	August 1963
Daily precipitation	Max.	63.7 mm	7.8.1984
Snow depth	Max.	86 cm	22.2.1966
Permanent snow cover (on average)	From	December 1st	1959 - 2000
	Until	March 5th	1959 - 2000
Duration of permanent snow cover	Min.	21 d	1959 - 2000
	Max.	181 d	1959 - 2000

There have been several past and ongoing studies in the same areas near the city center of Lahti. Some of those are part of this same project, while others are just topically related to this study. These research efforts have concentrated on e.g. stormwater runoff measurements from different types of urban areas (Valtanen et al., 2013), and detailed SWMM model parameterization and calibration (Krebs et al., 2013a).

4.2. Data

4.2.1. Publicly available spatial data

This study largely relied on publicly available spatial datasets. After the European Union established the INSPIRE directive, increasing amounts of such data have become available. Spatial data used in this study was mainly acquired from the National land survey of Finland (NLS, or *Maanmittauslaitos* in Finnish) through their open data file download service.

Orthophotos

The NLS provides color orthophotos with a terrain resolution of 0.5 meters (National land survey of Finland, 2013a). The orthophotos are aerial images that have been orthorectified to geometrically correspond with a map. These photos are a good reference for visual validation of other data and work well as a background for data visualizations. More detailed aerial photos would have been provided by the City of Lahti, but those were not needed as the NLS orthophotos proved to be adequate for this study.

Digital elevation model

The digital elevation model (DEM) provided by NLS is a raster dataset with a 2 m grid cell size (see Figure 6). Each grid cell contains a value for the mean ground surface elevation of the cell. The height accuracy is declared to be less than 0.3 meters. The dataset has been computed from airborne laser scanning data (see below) with a minimum point density of 0.5 points per square meter. Buildings are not depicted in the model. Instead, building cell values have been set according to a surface approximating the ground level at the site of the building. For this study, the digital elevation model 2 m was downloaded in ASCII Grid format from the NLS website (National land survey of Finland, 2013b).

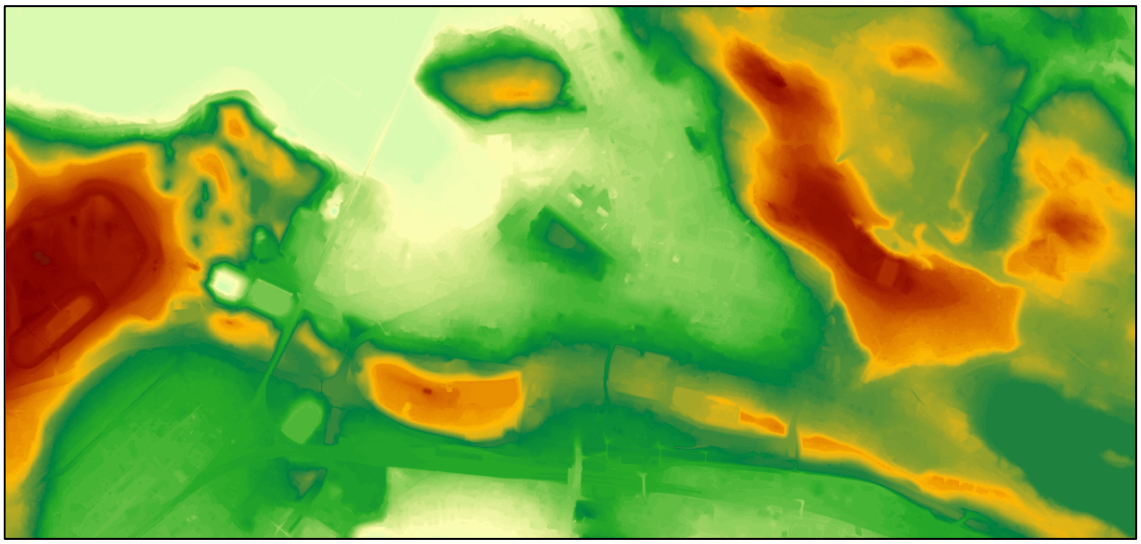

Figure 6. The digital elevation model (DEM). Hills are colored brown and red while lower lands appear green.

Laser scanning data

The NLS laser scanning data (see Figure 7) is a three-dimensional (x, y, z) point dataset representing the ground surface as well as objects on top of that surface. Points have been obtained by using an airborne LiDAR device transmitting laser pulses and sensing their ground reflections, coupled with accurate location information. Subsequently, the points have been classified mostly according to the LAS 2.0 format. Point categories include ground points, low vegetation points, water points, stream points, bridge points, etc. Points not suitable for any other classes are categorized as unclassified. Minimum point density of the processed points is 0.7 points per square meter. The data is provided for tiles of 3 km times 3 km. (National land survey of Finland, 2013c)

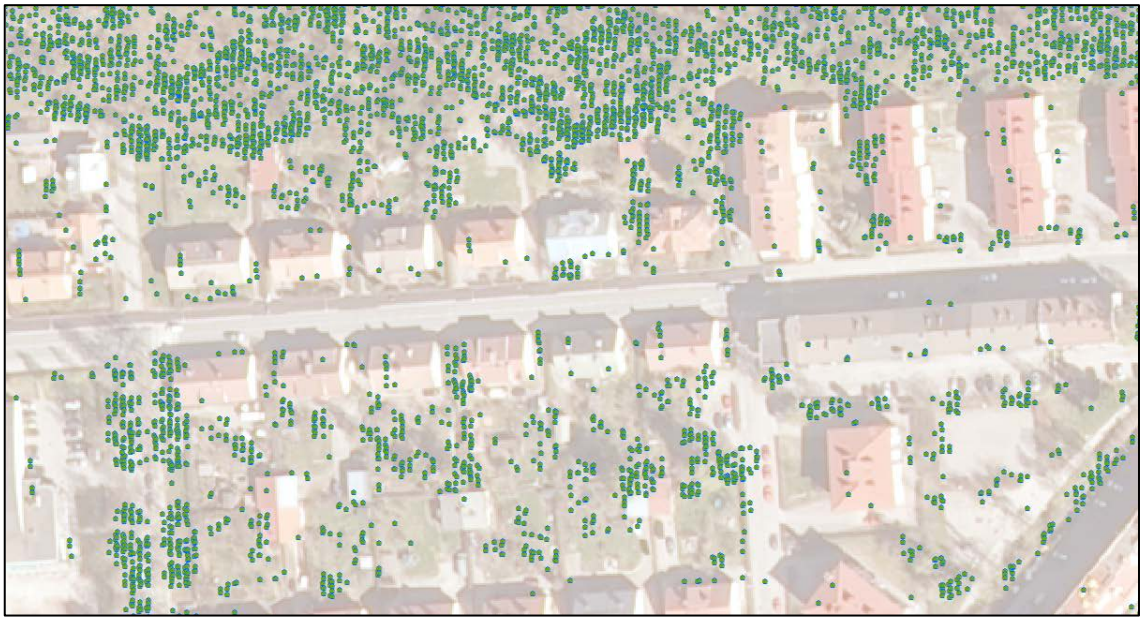

Figure 7. Laser scanning data, with only Class 3 (Low vegetation) points set visible on top of an orthophoto.

Topographic database

The topographic database (see Figure 8) of the NLS includes all types of objects that may appear on a typical base map. Each object belongs to a class such as traffic route networks, buildings & constructions, land use, water systems, elevations, and administrative borders. There are also sub-classes. For example, buildings are further classified according to the usage and the number of stories. Similarly, traffic route networks are classified as roads, streets, light traffic routes, railroads, etc. Streets and roads are stored in the database as linear features with a class number indicating width and the number of lanes. This is the most accurate nation-wide traffic route network dataset. (National land survey of Finland, 2013d)

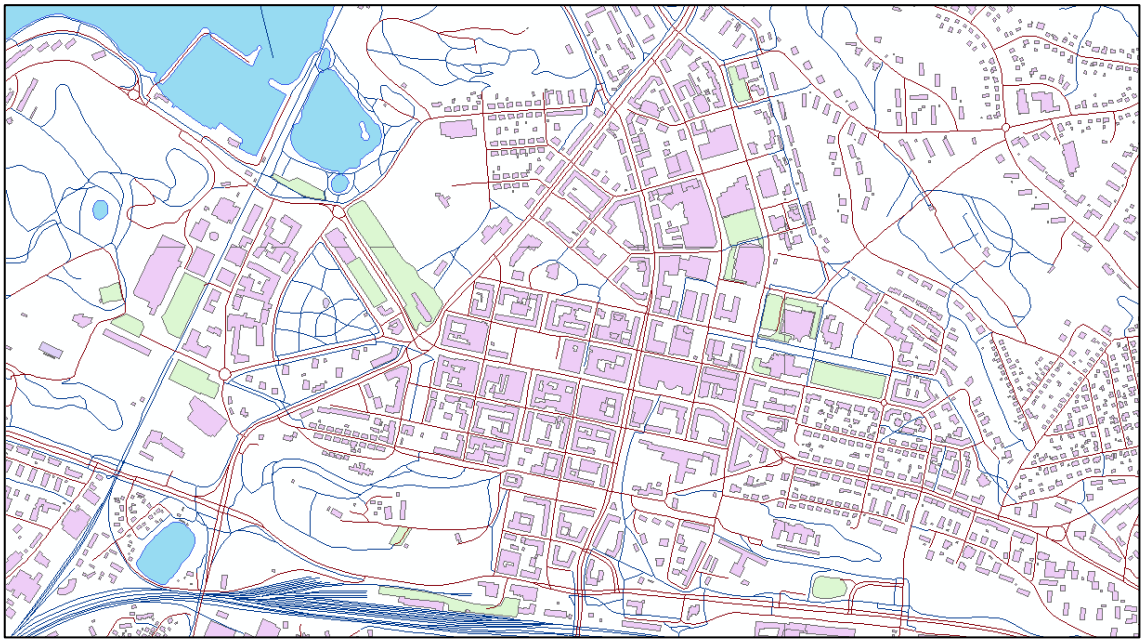

Figure 8. Some elements (buildings, roads, lakes, etc.) of the topographic database at the center of Lahti.

‘geoland2’ High Resolution Imperviousness Layer 20 m

The High Resolution Imperviousness Layer (see Figure 9) has been generated in the collaborative EU-funded project ‘geoland2’ (VITO NV, 2012). Several service providers are involved in the project, but for Finland the data was produced by Metria, a consulting company from Sweden. The HR Imperviousness Layer is a raster dataset with a cell size of 20 m. Cell values indicate the percentage of impervious cover in the cell area.

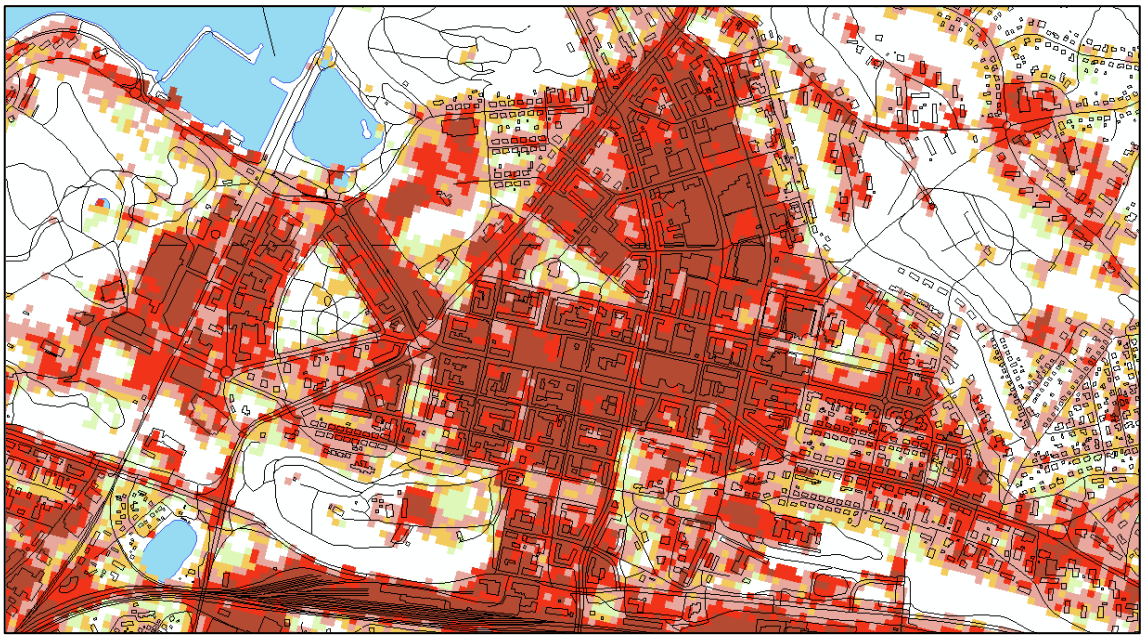

Figure 9. The HR Imperviousness Layer overlaid with elements from the topographic database at the center of Lahti. The cell colors indicate the imperviousness percentage (blank: 0 %, green: 1 to 20 %, yellow: 21 to 40 %, light red: 41 to 60 %, bright red: 61 to 80 %, and dark red: 81 to 100 %).

In this dataset, imperviousness is defined similar to soil sealing according to the FAO Land Cover Classification System (geoland2, 2009). Areas where the natural land cover has been substituted with an artificial, often impervious cover such as asphalt, metal, concrete, etc., or where soil is substantially compacted, are considered impervious (Di Gregorio, 2005).

The data is based on European Space Agency's Image2009 satellite images that have been resampled to a 20 m raster grid. To obtain the imperviousness degrees, the land surface has been automatically classified based on calibrated normalized difference vegetation index (NDVI). The results of the automated process have also undergone visual review and improvement. Data validation has shown that the geometric accuracy of the data is less than 30 meters. Additionally, the thematic accuracy of the data has been assessed by studying cell classification as built-up cells (with imperviousness of at least 80 %). In Finland, the data has overall thematic accuracy of 97.4 % for recognizing the built-up cells. Some commission error still exists, implying that the calculated imperviousness values may be higher than in reality. (geoland2, 2010; Maucha et al., 2011)

4.2.2. Stormwater system layout

Data describing the properties of the stormwater system was received from Lahti Aqua Oy, the local water supply company in Lahti area. The data (see Figure 10) had been imported into ESRI shapefile format assumingly from the company's Tekla Xpipe database. The data received consisted of several feature classes, including:

- stormwater drains (as polyline features);
- manholes and pipe junctions (as point features);

– attribute data belonging to nearby features (as point features).

Figure 10. Part of the stormwater drainage network data. Only 'real' features are shown on the map, and point features containing attributes of these 'real' features are not visible.

In other words, most of the necessary information such as pipe diameters, pipe elevations, and manhole elevations, was not attributed to the objects forming the drainage network, but to separate point features in the proximity of the actual network objects. Several objects also completely lacked some or all of the basic attributes required for model parameterization, and there were occasional gaps in the geometrical continuity of the drainage network. Furthermore, many pipes appeared to have imaginary duplicates in the data. The features on the private properties and the ones on the street area had typically been stored in corresponding different feature classes. Overall, in terms of its quality the data was not well-suited for the purpose of this study.

4.2.3. Weather observations data

Weather data was obtained from the Finnish Meteorological Institute (FMI). The data includes observed values for air temperature [°C], relative humidity [%], wind speed [m/s], precipitation [mm], and snow depth [cm] at the Laune meteorological station in Lahti. The recording interval was 3 hours, expect for precipitation for which hourly records existed. The time period covered by the observations is nearly four years, from 01/01/2008 to 11/21/2011. The data has been pre-processed as described by Krebs et al. (2013a).

Annual precipitation shows great variability during the observation period. Wet year 2008 was record-breaking throughout Finland (Finnish Meteorological Institute, 2008), including Laune with an annual precipitation of 896 mm. The following three years the value remained lower, around 600 mm per year. Monthly precipitation during this period is presented in Figure 11.

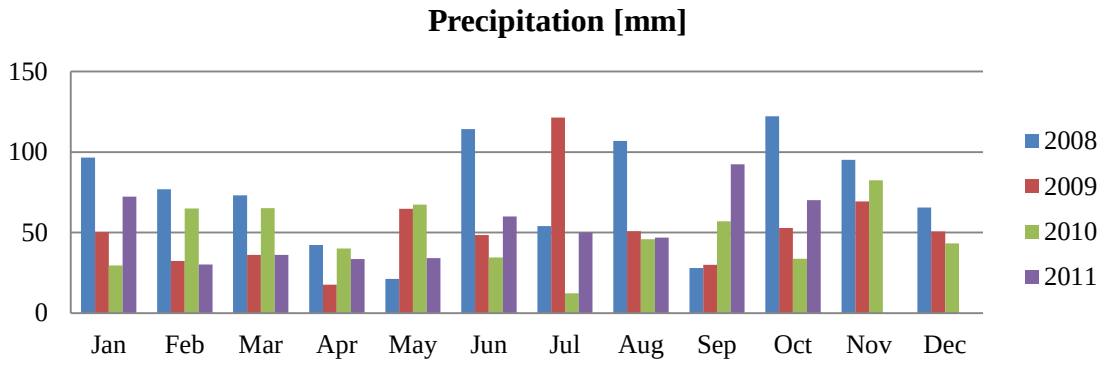

Figure 11. Monthly precipitations at Laune from January 2008 through October 2011.

According to FMI (Finnish Meteorological Institute, 2013), the Laune meteorological station (WMO station identifier 02965) lies in the Porvoonjoki river valley 83 m AMSL. The station is located in a garden in a family house area. The First Salpausselkä, a major ridge of glacial origin with its top at 150 m AMSL, rises two kilometers north from the station (see Figure 12). The surroundings of the meteorological station consist of wide natural fields and forested hills. Wind speed is measured at the height of 12 m and is possibly affected by some nearby trees and buildings.

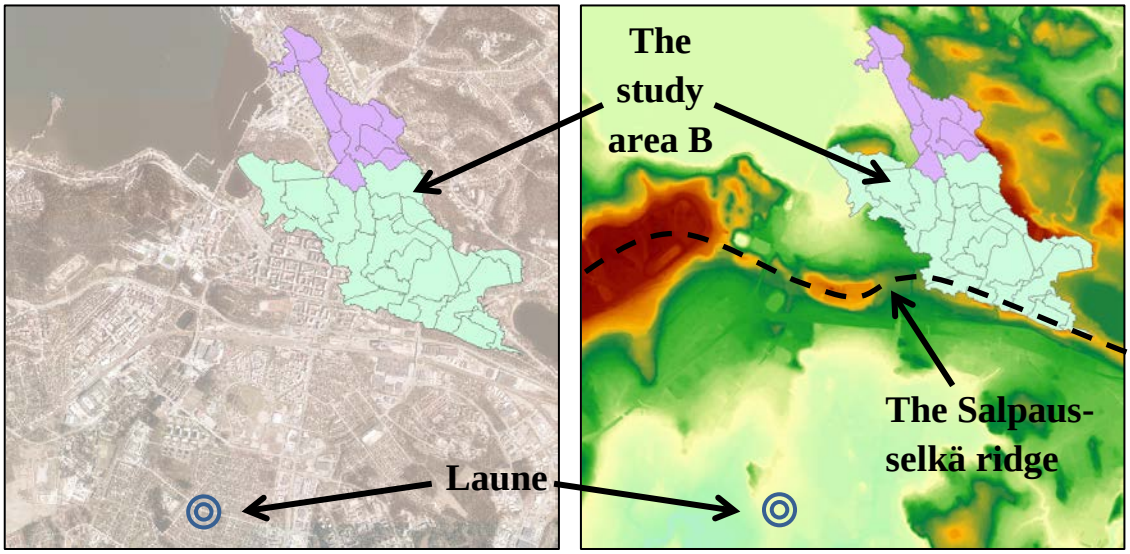

Figure 12. Location of the meteorological station relative to the study area.

It is reasonable to slightly question the suitability of weather data from Laune to describe the weather conditions in the study area. According to a local meteorologist at FMI (Kaukoranta, 2012), the Laune neighborhood is characteristically colder than the city center of Lahti. Laune is less densely built and thus the urban heat island effect plays there a reduced role. Also, Laune is located in the river valley at a level approximately 20 meters lower than the city center, and the Salpausselkä ridge induces different microclimates on each side of the ridge. On a clear and calm weather, the measured air temperature in the city center may be even 3 to 4 °C warmer than at Laune. A new meteorological station is actually planned to be installed in the city center to achieve weather forecasts better representing the city area.

5. RESULTS AND DISCUSSION

5.1. Catchment and subcatchment delineation

One objective of this work was to identify a catchment delineation that supports SWMM modeling in the city of Lahti. First, a coarse catchment delineation was performed for study area A. Thereafter, a more detailed delineation and catchment subdivision was performed for study area B which was prescribed based on the coarse catchment delineation.

Input data used in the catchment delineation process included the DEM and the stormwater system layout data. In addition, some orthophotos and Google Street View images were used to aid visual validation of the results.

5.1.1. Preliminary catchment delineation of study area A

The two-meter DEM was used to identify and delineate all catchments draining into Lake Vesijärvi in the Lahti municipality area. To begin with, a depressionless DEM was created using the ArcGIS *Fill* tool (Esri, 2012). The *Flow Direction* tool (Esri, 2012) was applied to the depressionless DEM to create a flow direction grid (FDG). This tool utilizes the D8 method (Fairfield and Leymarie, 1991) for determining the surface flow direction from each cell to one of its neighboring cells. In the FDG, every cell has a value indicating the direction of the flow leaving the cell. Then, a flow accumulation raster (FAC) was created using the *Flow Accumulation* tool (Esri, 2012). Each cell in the FAC is assigned a value indicating the number of upstream cells contributing to the flow through that specific cell. Cells with high flow accumulation values thus are typically parts of the stream network in the area in question.

Next, the symbology of the FAC was set such that only the cells over a threshold value of 2500, corresponding to a contributing area of 1 hectare or more, were visible. This enabled overlaying the streams of the FAC and the streams from the topographic database (width > 2 m) for visual inspection (see Figure 13). Two interesting notes were made: (i) stream features of the topographic database rarely appear in the city center, although FAC implies they exist; and (ii) a typical cause of error in the stream location was that culverts are not represented in the DEM. In case (ii), the *Fill* tool often raises surface elevations in the area upstream of the culvert until the water finds its way over the road, often at location other than the real culvert location. Areas where erroneous depression-filling occurred were listed in order to keep track of the need for further processing. These areas were localized using raster algebra for subtracting the original DEM from the depressionless DEM produced by the *Fill* tool. Areas with a clear difference were in most cases those draining through culverts not represented in the DEM.

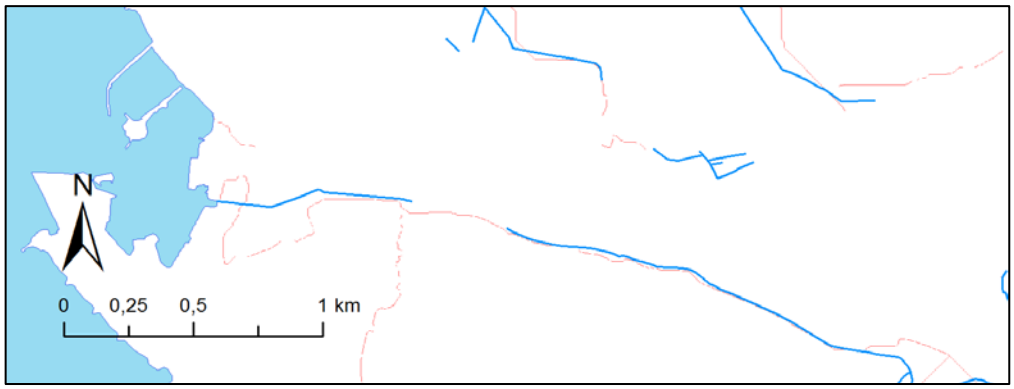

Figure 13. Comparing the streams from FAC (red) against streams from the topographic database (blue).

The visualization of the stream network in the FAC allowed for the determination of the streams draining into Lake Vesijärvi in or within a close distance to the Lahti municipality area. New point features were digitized approximately 10 meters upstream from the locations where each of the streams entered Lake Vesijärvi. Altogether, 72 pour points were created in the Lahti area and 7 in Hollola area (the neighboring municipality). The *Snap Pour Points* tool (Esri, 2012) with a 5-meter tolerance setting was used to assure all the pour points created were correctly positioned at a stream cell.

Finally, the *Watershed* tool (Esri, 2012) was used to identify catchments contributing to the flow at each of the pour points. The tool creates a raster where cell values indicate to which pour point cells are draining to.

Visual comparison was carried out to observe the similarities and differences of the catchment delineation and the stormwater drainage network layout (see Figure 14). In a few places, the stormwater drains crossed the catchment borders. This is one signal that catchment delineation of an urban area should not solely base on terrain topography but should also consider the stormwater system.

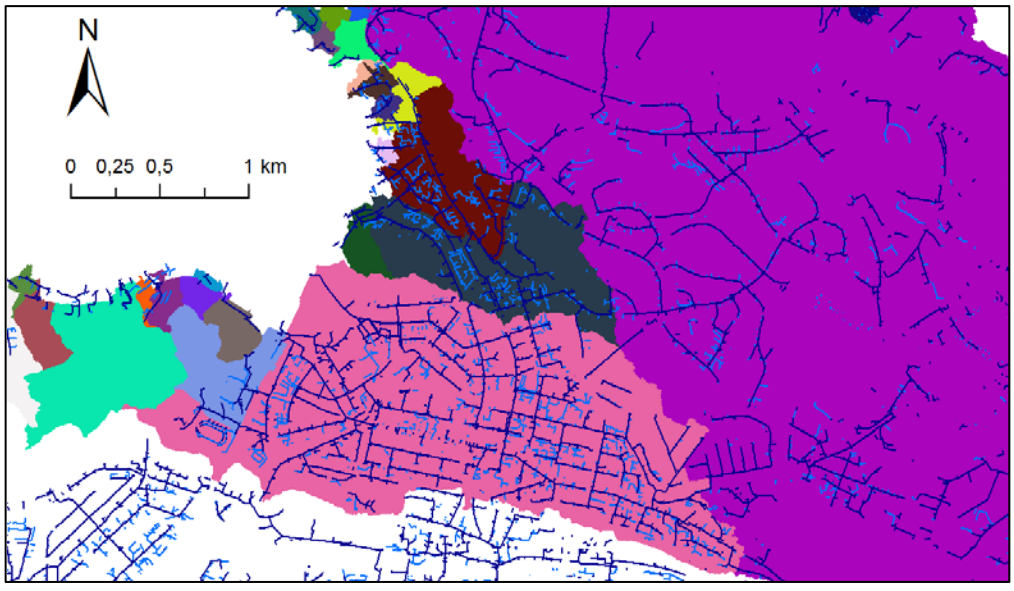

Figure 14. Preliminary catchment delineation (colored areas) overlaid with stormwater drainage network layout for visual comparison. The light blue lines represent stormwater drains on the properties while the darker blue lines are larger pipes typically located under the street area.

5.1.2. Detailed catchment delineation of study area A

The use of DEMs for watershed and stream delineation in urban areas results in stream networks not correspondent with reality due to the negligence of the stormwater sewer network and flow obstructions. This issue can be avoided by incorporating vector stream or sewer data to complement the original DEM. In the technique called 'stream burning' the elevation of cells representing a stream or a section of the sewer network is reduced to ensure that the flow is never leaving the channel but following it all the way to the pour point (Saunders, 1999).

According to Callow et al. (2007), stream burning replicates catchment area and stream length quite fittingly. However, mean and maximum channel slopes may be increased.

As noted from the coarse catchment delineation above, missing culverts and inter-catchment drainage lines were potential error sources in the delineation. To produce a more detailed catchment delineation stream burning was thus involved.

The stormwater network was combined with the natural streams from topographic database to create a complete stream network vector dataset for burning. Validity of this data was checked visually and corrections were made where needed. Special attention was paid to places of flow bifurcation as those would have caused problems later in the delineation process. Some examples of corrections made are:

- Near Lake Pikku-Vesijärvi pipes formed a complex network covering a rather flat area of ca. 2 hectares where the flow directions for each pipe were ambiguous. The diameters and inlet and outlet elevations of the pipes indicated that some of the pipes were designed for overflow situations only. Consequently, they were discarded for the normal catchment delineation.
- Some distance north from Lake Joutjärvi there was an overflow drain in one of the manholes, implying that the upstream area could be drained into one of two different catchments. The overflow pipe connection was manually deleted.
- There is a traffic tunnel through Mustakallio hill having some kind of drain going through it. This drain needed to be disregarded for two reasons: (i) it falsely connected the two catchments on either side of the hill, and (ii) if burnt into the DEM, it would have collected runoff from top of the hill, which obviously is not realistic.
- At two distinct locations, two pipes seemed to cross each other on vertically different levels. For both locations, the other pipe was found to be of little significance and could be manually edited to allow all the water to flow into the major drain.
- Numerous culverts were added at locations listed in the coarse delineation process above.
- The culvert draining Lake Merrasjärvi was extended to prevent the *Fill* tool from filling the whole lake by 40 cm.

In reality, bifurcation can be found both in natural streams and stormwater sewers. Nevertheless, all the above corrections were judged to cause only minor errors. And if any resulting error would later have proven substantial, the bifurcation could have been implemented again in the SWMM model structure.

To achieve a correct catchment delineation, all sinks noted in the coarse delineation phase needed to be drained by burning the DEM with culverts and stormwater drains. The only exceptions could have been depressions that also in reality are areas of internal drainage, e.g. kettle holes. No surface runoff is formed on such areas but all excess water is either evaporated or infiltrated. Although kettle holes exist in Lahti, the DEM showed there were none of them in the study area B described below.

The stream network data was converted into raster format using the *Polyline to Raster* tool (Esri, 2012). Cell size was set to 2 m and the raster grid was snapped to the DEM. The streams were burnt into the DEM by setting stream cell elevation to zero using the *Raster Calculator* tool (Esri, 2012) with the expression: *Con(IsNull("Stream_raster"), "DEM_raster", 0).*

Next, the *Fill* tool (Esri, 2012) was used to remove depressions from the burnt DEM. The sinks filled by the tool were examined using the same method as above. Where major sinks had been filled, additional culverts were burnt into the burnt DEM. After this, the *Fill* tool was again used for the updated DEM. This process was iterated for a few times until no major sinks existed in the burnt DEM.

Thereafter, the procedure was similar to the preliminary delineation phase. The only difference was that the threshold value was this time set to 12 500 cells (or 5 hectares), resulting in 33 catchments (see Figure 15).

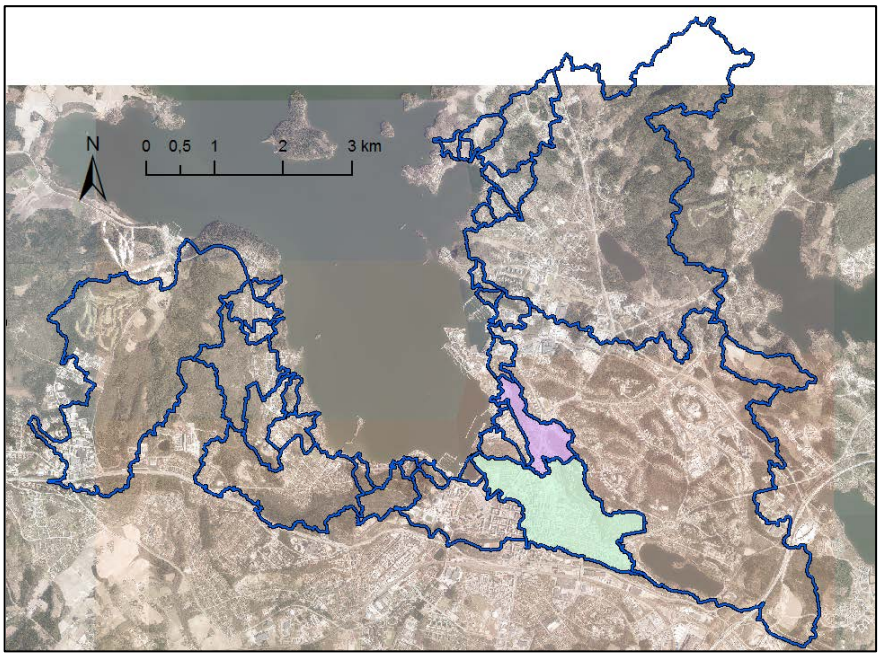

Figure 15. Detailed catchment delineation for the study area A. Blue lines represent catchment borders. Colored areas indicate the study area B (see below).

5.1.3. Selecting the area for closer study (study area B)

The next objective of the study was the subdivision of the catchments delineated above. For the purposes of testing SWMM in this work, the study area was reduced compared to the previously defined study area A. One of the reasons for this was the excessive amount of manual work required to make the stormwater network data usable in a large extent.

The new geographic scope was set to cover two catchments in the center of Lahti (see Figure 16). These particular catchments were chosen because in these areas:

- there were ongoing studies by Krebs et al. (2013a; 2013b) on two of the subcatchments;
- no combined sewers existed;
- stormwater sewer pipe data was of rather good quality.

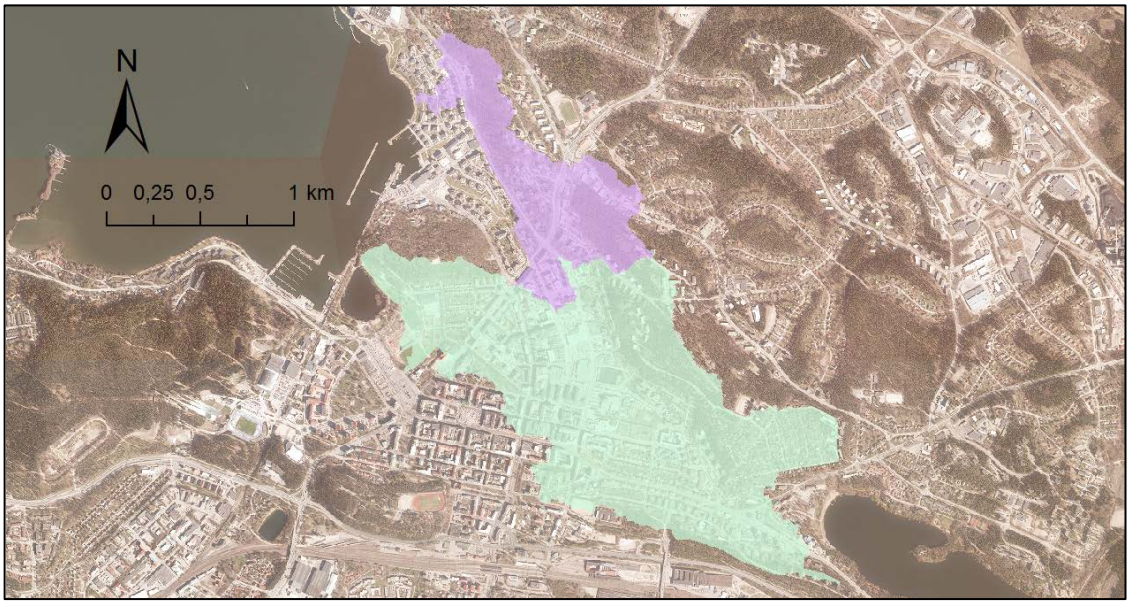

Figure 16. Study area B, consisting of two neighboring catchments (colored green and purple).

5.1.4. Catchment subdivision for study area B

To allow for a sufficiently detailed SWMM model structure, the study area B had to be divided into subcatchments. The appropriate subcatchment area was defined at ca. 5 hectares to maintain comparability with the results of Krebs et al. (2013a; 2013b), who conducted detailed SWMM parameterization in areas of the same size class.

Subdivision can be performed in ArcGIS by introducing additional pour points along the streams within a catchment. Several methods for adding these pour points were considered: (i) based on the stormwater system layout and diameters, (ii) based on the flow accumulation grid, or (iii) manually on a case by case basis. The last mentioned was considered only as a backup option in case the two others would fail.

Possible differences between methods (i) and (ii) were studied by comparing the relationship of pipe diameters to flow accumulation values. As pipe polyline data had no attributes, diameters had to be imported from another point dataset, partly using the *Select by Location* tool (Esri, 2012) and partly manually. To limit the work, this process was performed only for diameters equal to or greater than 500 mm. As some diameters were non-existent even in the point data, they needed to be interpolated from up- and downstream values. The network of pipes with a minimum diameter of 500 mm was then overlaid and visually compared with the streams of FAC using the threshold of 5 hectares (see Figure 17). In the majority of locations, the FAC stream continued further upstream than the 500 mm pipe.

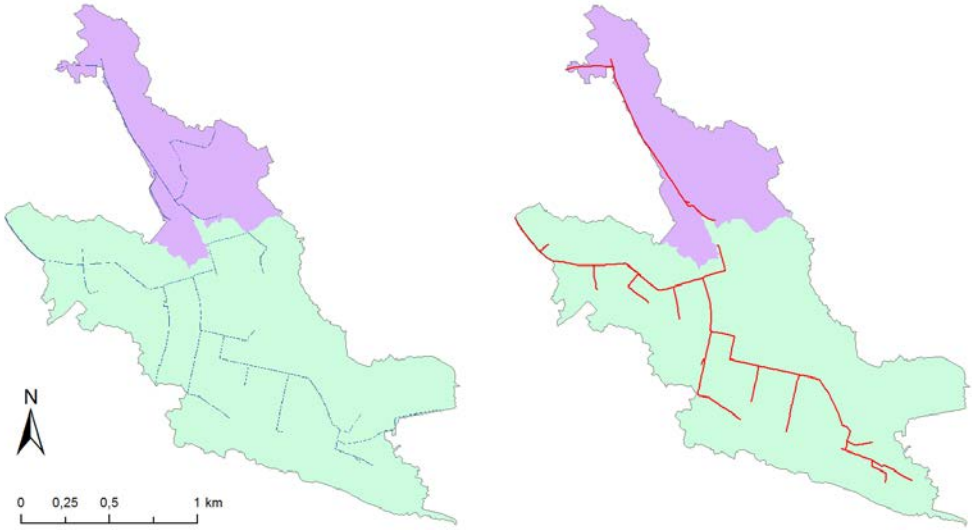

Figure 17. Flow accumulation grid with a 5 ha threshold (left) and stormwater drains with a minimum diameter of 500 mm (right).

Due to the poor quality of the pipe data, the method based on the FAC values was judged to be a better starting point for the subdivision of large catchments. The threshold value was retained at 12 500 cells (5 ha), and all FAC cells not exceeding the value were set null with the *Raster Calculator* tool (Esri, 2012). The *Stream to Feature* tool (Esri, 2012) was next used to create a polyline feature class representing the stream cells as a network.

It was obvious that setting a pour point at the upstream end of each stream would result in upstream subcatchments of precisely 5 ha, just as wanted. The interesting question was how to locate pour points for those subcatchments that had one or more contributing upstream subcatchments. A principle thus experimented was to add an intermediate pour point at every location where two or more FAC 5 ha threshold streams meet. Both the upstream and the intermediate pour points could be created with the *Feature Vertices to Points* tool (Esri, 2012) with the point type set as 'Both ends'. The original downstream outlet points of the whole catchments were then merged to the pour point dataset, and all the points were again snapped to the streams using the *Snap Pour Point* tool (Esri, 2012). Finally, the subcatchments could be delineated with the *Watershed* tool (Esri, 2012). After viewing the results, some subcatchments of the size

of just a couple of cells were manually merged with their larger neighbors. In addition, one subcatchment was dropped out of the scope as it is drained by combined sewers, according to the pipe layout data and Lahden seudun ympäristöpalvelut (2010). The pour points and corresponding subcatchments are shown in Figure 18.

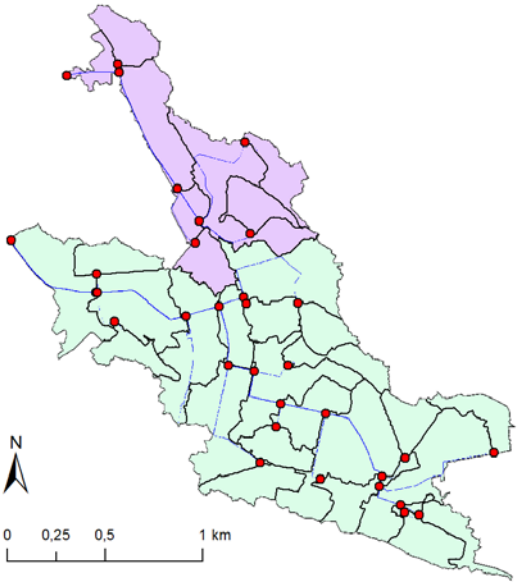

Figure 18. Pour points (red dots) and subcatchment delineation (black lines). Flow routes are presented blue.

The size distribution of the subcatchments was plotted to ensure the sensibility of the delineation. Some of the subcatchments were of the size of only one or two raster cells (4 to 8 m^2), and were simply removed from the data. In addition, one tiny subcatchment of 0.17 hectares was merged to its greater upstream neighbor. The size distribution of the final subcatchments after these operations is presented in Figure 19. Approximately half of the subcatchments are close to the areal target of 5 hectares, while 13 % are considerably smaller and 34 % are considerably larger.

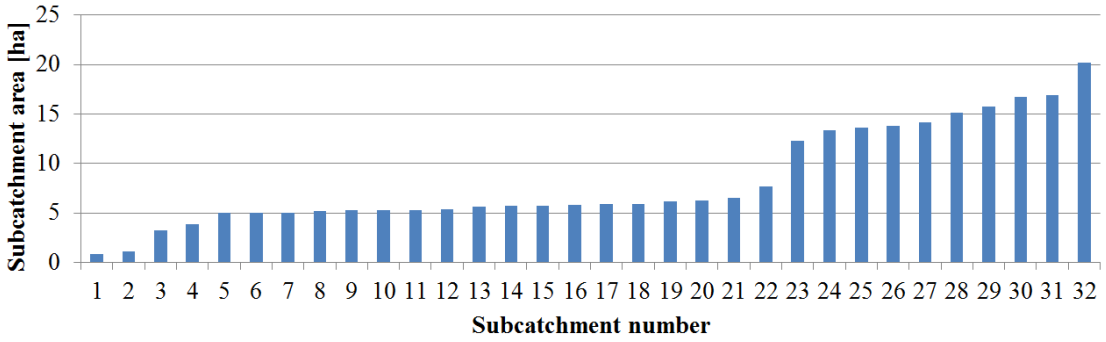

Figure 19. Size distribution of the 32 subcatchments.

The method of setting pour points at all junctions of major pipes seems to have produced subcatchments with an area often triple or even quadruple of the desired. For this study area, an appropriate measure could have been to set the pour points as above, but split the subcatchments along the main sewer lines so that each side of the main sewer is a separate subcatchment.

In the first place, the intention was to also experiment with other subcatchment threshold values. This was judged too laborious for two reasons: (i) Increasing the number of subcatchments would have required more pre-processing of data on small pipes. (ii) While the size of the upstream subcatchments could easily have been altered by changing the pour point threshold, the intermediate and downstream subcatchments would still have remained the same, unless pour points had been manually created along the pipe sections between junctions.

As told in Chapter 2.2.2, subcatchments in an SWMM model should be internally homogeneous in terms of e.g. land-use and surface materials. With the delineation method employed here one can be sure that that is not the case. One of the aims of the next chapter is to find out whether it is possible to choose justified parameter values for such heterogeneous subcatchments.

5.1.5. Summary of catchment delineation and subdivision

To validate the results of the catchment delineation and subdivision, comparison was made with the catchment delineation conducted by Krebs et al. (2013a; 2013b). They performed detailed catchment delineation based on field observations on two of the subcatchments of this study. In Figure 20 one can see that they have set their pour points slightly further downstream (representing the last stormwater sewer inlet before the runoff measurement station) from the pour points of this study. This results in a difference in the shape and size of the subcatchment shown on the right in Figure 20. Another major dissimilarity is in the northern limb of the subcatchment shown on the left of Figure 20. The difference is caused by runoff from a steep hill flowing over a flat street area with such high velocities that the street inclination is not sufficient to guide all the water into the drains at the sides of the street, like should happen according to the DEM.

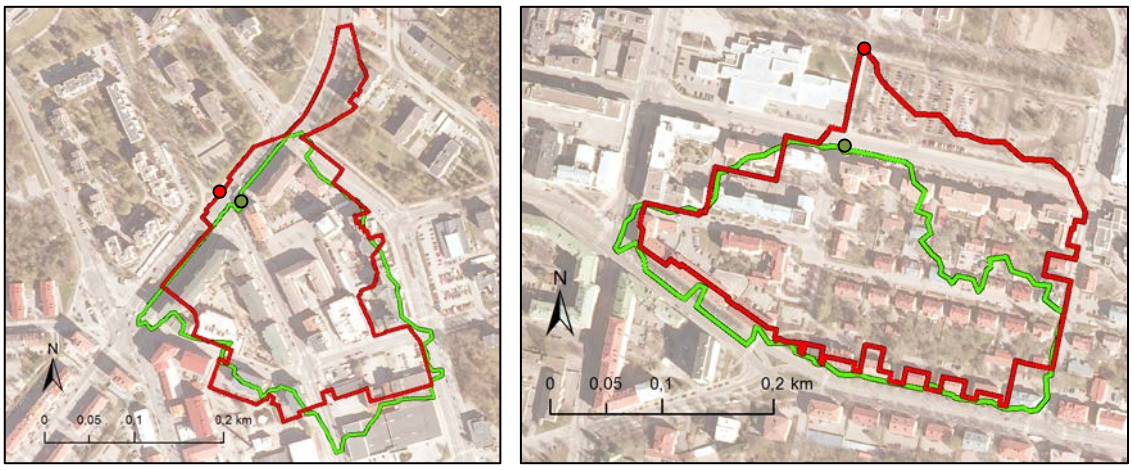

Figure 20. DEM-based subcatchment delineation (green) compared with the detailed delineation (red) by Krebs et al. (2013a; 2013b) on two of the subcatchments. Subcatchment pour points are marked with dots.

Despite the two larger dissimilarities, the subcatchment delineation performed in this study corresponds with the results of Krebs et al. (2013a; 2013b). Most differences

occur on a building scale. Those could possibly be avoided by doing the above analysis based on a DEM with building data included, such as the one created in Chapter 5.2.4.

Overall, based on the results of this study, catchment delineation of an urban area should build both on (i) terrain topography as well as (ii) detailed and comprehensive data of the stormwater drainage system. Urban catchment delineation and subdivision is an iterative process that cannot be fully automated due to regular deficiencies in the data.

Manual work is always necessary to review the quality of the drainage network data and make corrections where needed. For a large area, data is likely to be insufficient to some extent. A typical cause of delineation error is that all culverts do not appear in the pipe network data but need to be added manually.

Setting subcatchment pour point locations is a critical part of the subdivision process. The problem is that there is no one right way of doing it. The method for choosing pour points used in this study was straightforward to apply but is nonflexible in terms of creating subcatchments of a certain desired size class.

A couple more things must also be noted regarding the methods used: (i) Burning the stormwater drains in the DEM includes the assumption that water could enter the drain at any point along its course. Naturally this is untrue for all pipe flow, as the runoff may in reality enter only through inlets such as manholes etc. (ii) Some locations of sewer-flow bifurcation were omitted in the model. Existence of such details however implicates that the catchment delineation is ambiguous. In other words, runoff from certain areas could actually end up in two separate destinations depending on the state of the system. (iii) Due to sandy soil and hilly topography, it is likely that horizontal surface-layer and ground-water flow occurs at the study area. As flow within the soil might head in different directions than on the surface, the catchment delineation performed here applies only for the surface flow. To conclude, the above three aspects prove that the catchment delineation performed in this study is only a mere approximation.

5.2. Subcatchment parameterization

Subcatchments require a wide range of parameters until they can be modeled in SWMM. Some of these parameters (e.g. subcatchment area) are easier to obtain, although uncertainties may be involved. In contrast, other parameters (e.g. flow width) require complicated GIS processing to reach even rough estimates. One of the objectives of this study was to develop parameter estimation methods and to evaluate their applicability to large areas with the data sources typically available.

Before going into detail on the subcatchment-specific parameters, some general parameter settings are mentioned: (i) each subcatchment was manually assigned to a correct outlet node in the drainage network, (ii) subcatchments were named with numbers corresponding to the outlet node numbering, (iii) runoff from both the pervious

and impervious fraction of a subcatchment was set to be routed directly to the outlet, and (iv) all subcatchments were linked to the same rain gage at Laune.

5.2.1. Imperviousness

The imperviousness parameter describes the percentage of impervious surfaces in relation to the total area of a subcatchment. It is often used as a calibration parameter (Choi and Ball, 2002) as it is not quite straightforward to physically define, due to e.g. the fact that many surfaces are in reality partially impervious. For this study, no flow measurements were available, and therefore calibration was not an option. Other ways to define the values of imperviousness are to estimate them based on land use data, or by automated or manual image processing of aerial or satellite orthophotos.

In this study, the geoland2 High Density Imperviousness Layer (see Chapter 4.2.1) was used for subcatchment parameterization. The raster was projected into the Finnish coordinate frame EUREF-FIN using the *Project Raster* tool (Esri, 2012), and the output cell size was simultaneously reduced to 2 meters. Next, the mean imperviousness (see Figure 21) was calculated for each of the subcatchments with the *Zonal Statistics* tool (Esri, 2012), and these values where set as attributes of the subcatchment features.

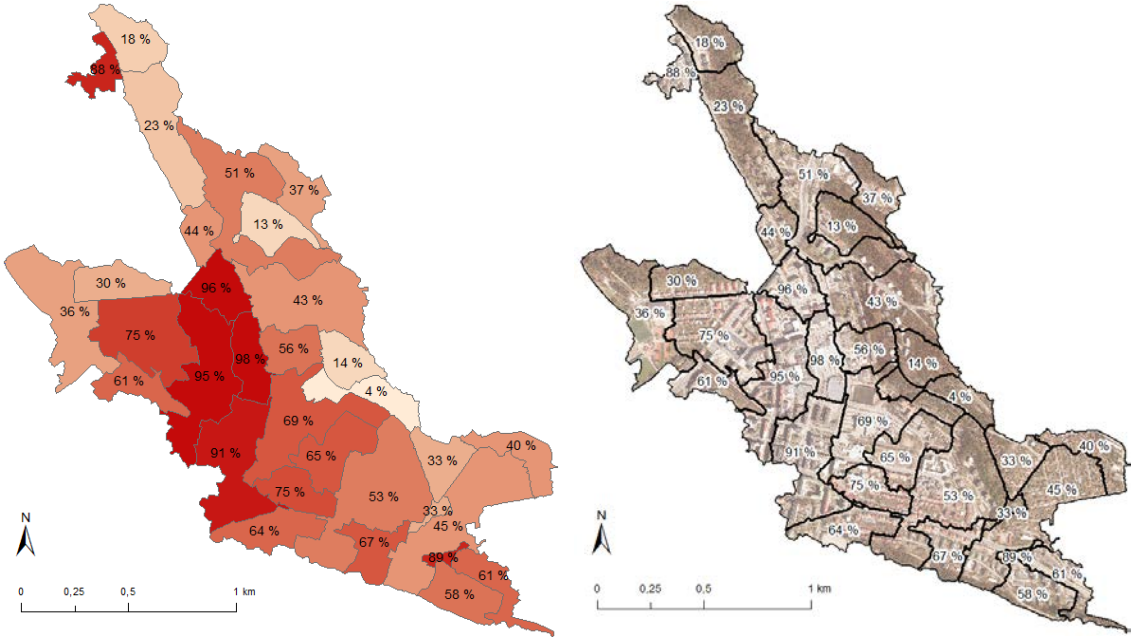

Figure 21. Subcatchment imperviousness values used in model parameterization.

Visual comparison with aerial orthophotos instantly showed that imperviousness values gained were in the appropriate order of magnitude. Chapter 5.2.8 provides a more detailed summary of the results.

Before using the geoland2 data, the first approach in this work had been trying to define imperviousness through combining land use information from the topographic database and some other sources. The aim was to sum up all the impervious and pervious features in the subcatchments. To begin with, the topographic database contains several types of polygons that can quite safely be assumed to be impervious. These include

different types of buildings, as well as some (but not all) parking lots. Other major impervious area types include roads and streets that also are depicted in the same database. However, they are presented only as centerline-presenting polyline features, with attributes telling their supposed widths. These width attributes were utilized to create an appropriate buffer around the centerlines, but visual comparison against orthophotos showed that the result was poor. The width attributes of the database varied considerably in relation to the width visible in orthophotos. In addition, sidewalks were not shown in the database.

The topographic database contained practically no usable data on pervious areas. For that reason, possibilities of the laser scanning data to describe pervious areas were also studied. The data was imported from the LAS format to a point dataset in ArcGIS geodatabase format so that only point class 3, 'Low Vegetation' was included. Visual comparison against orthophotos showed that the laser points represented mainly trees. This suggested that areas with dense points were supposedly pervious. Different buffers were applied to see which would turn the points into the most representing pervious polygon features. In forested areas this seemed to be a suitable technique.

The problem with this first approach was however that after including the above described polygon features, a large portion of the subcatchments still remained empty. In an urban area there are several sub-areas, such as the lawns, that are not presented by the above data classes. Therefore, a different approach was needed.

A second option could have been incorporating automated image processing such as spectral analysis. A technique called Normalized Difference Vegetation Index (NDVI) has been successfully used for this kind of tasks; see e.g. Montzka et al. (2006). However, this method was not studied further as the results based on the geoland2 data seemed adequate for the means of this study.

5.2.2. Depression storage

SWMM treats the pervious and impervious parts of a subcatchment separately, and thus both may be given independent values of depth of depression storage. One can also define a portion of the impervious area to have no depression storage at all. This could be realistic on steep roofs, for example. The SWMM User's Manual (Rossman, 2010) suggests some literature values for the depression storage. For impervious areas, the values range from 1.3 to 2.5 mm, and for lawns from 2.5 to 5.1 mm. The highest value is given for forest litter (7.6 mm). These values are not very exact, and depression storage actually is one of the common calibration parameters used for SWMM parameterization (Choi and Ball, 2002).

Based on the values above, the depression storage for all subcatchments were set to 1.9 mm for impervious subcatchment fraction and to 5.1 mm for the pervious fraction. The percent of impervious area without depression storage was set to zero. The values are compared with calibrated values by Krebs et al. (2013a; 2013b) in Chapter 5.2.8.

5.2.3. Infiltration

The Green-and-Ampt model used by SWMM to account for infiltration involves two soil-dependent parameters: (i) capillary suction head ψ, and (ii) saturated hydraulic conductivity K. In addition, the initial state of the infiltration model is defined by a third parameter, the initial moisture deficit *IMDmax*.

Infiltration parameters depend on the soil type. The surficial deposit map of Finland (Geological Survey of Finland, 2013) offers no data coverage for the built areas in the city center of Lahti. However, one can assume those areas to resemble their surroundings, indicating sand and till would be the dominant soil types within the study area B. Typical infiltration parameter values for sandy soils are presented in Table 3 below.

Table 3. Literature values for infiltration parameters (Rossman, 2010).

Symbol	Variable	Unit	Value for sand	Value for loamy sand	Value for sandy loam
K	Saturated hydraulic conductivity	mm/h	120	30.0	10.9
ψ	Soil suction head	mm	49.0	61.0	110
φ	Porosity	-	0.437	0.437	0.453

As the infiltration parameters should reflect the properties of the often loamy surface-soil layer, the values given for sandy loam were considered most appropriate. For the initial moisture deficit parameter Rawls et al. (1992) give maximum values from 0.35 for sand to 0.25 for sandy loam. Using these values as such depicts the soil as efficiently drained, implying that ground water would not limit the infiltration. This is assumingly not always true, but in the absence of better knowledge *IMDmax* was still set to the value of 0.25.

5.2.4. Slope

In SWMM subcatchments are conceptually represented as rectangular planes. These planes are inclined so that all surface flow is directed perpendicularly towards one of the edges of the rectangle. The slope parameter tells the amount of inclination.

In reality, the subcatchment shape and slope vary within the subcatchment. This is the case especially with large heterogeneous subcatchments like those of this study. Thus, the most feasible way to derive subcatchment slopes would be to calculate them from DEM.

Considering the model conceptualization, the composite slope of a subcatchment should be based on the slope along the flow paths in the subcatchment. This could be achieved by calculating the slope at each cell to the D8-derived flow direction from that cell. Unlike in the conceptual model, flow is concentrated in the stream cells while numerous upstream cells transfer only small amounts of flow. For this reason, the cell-by-cell slope should be weighted by flow accumulation before averaging over a subcatchment.

Obviously, the burnt DEM is not a proper input for slope calculations, as the drop into the burnt channels would produce unrealistic slopes in the cells along the channels. The question remains whether the original DEM or the depressionless DEM produced by the *Fill* tool (Esri, 2012) would be more suitable for the slope assessment. The latter may be a little flatter which may affect the results. Here, the original DEM was used as a starting point. From the perspective of slope there is though one major flaw in this data: the buildings have been erased from the terrain. Omitting buildings probably unrealistically reduces the average slope, as many rooftops are areas with large slopes.

To account also for the buildings, those needed to be added into the DEM. First, laser scanning point data was imported to ArcGIS using *LAS to Multipoint* tool (Esri, 2012). Only points of class 1, 'unclassified', were imported. These points were clipped with the topographic database building polygons as clip features, so removing all points that were not located within buildings. The points were then stored in a single part format, and the *Point to Raster* tool (Esri, 2012) with the cell assignment method set as 'mean' was used to create a DEM describing the building rooftop elevations. These building cells were then mosaicked (see Figure 22) with the original DEM to create a complete representation of the terrain with buildings included.

Figure 22. Mosaicking the original terrain DEM (left) with the building DEM (center) resulted in a complete DEM (right).

ArcGIS offers two different methods of creating a slope raster with cell values indicating terrain slopes at each cell. The first one is the *Slope* tool (Esri, 2012), which employs elevations of all 8 neighboring cells to calculate the slope at a specific cell. This method was tried but judged possibly misleading, as the point of interest was the slope only in the direction of flow. The second practical method would have been using the drop raster produced by the *Flow Direction* tool (Esri, 2012). However, visual inspection showed that the drop raster values were not similar to what was expected based on the tool documentation. It seems there might be a bug in the ArcGIS algorithm.

As existing ArcGIS tools did not fit the task at hand, a custom-made script was used. The complete DEM was exported into ASCII format and opened in Microsoft Excel software. A Visual Basic script (see Appendix A) was run to calculate the slope on a

cell-by-cell basis. For each raster cell, the script calculates as a percentage the slope from the cell itself to that neighboring cell were the D8 algorithm would route the flow. The slopes obtained were then imported back into ArcGIS and are shown in Figure 23.

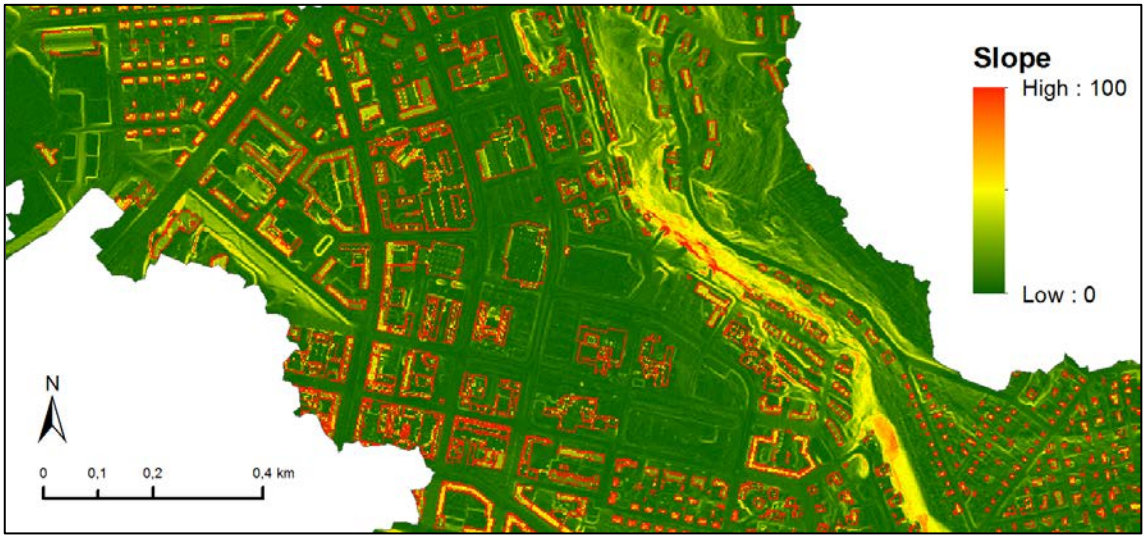

Figure 23. Slope raster showing extremely high slope values at rooftop edges.

Buildings cause remarkable vertical discontinuities in the terrain profile. Hence, the slope at a roof cell may be even hundreds of percent in case the flow is directed onto a cell on the ground next to the building. Such cells with extraordinary slopes seemed common in the urban area. If left unchanged, they would have unreasonably increased the mean subcatchment slopes. Using those extremely high slopes in SWMM would not be conceptually realistic, as increasing the local slope after a certain point mainly affects the energy loss due to turbulence, thus not shortening the response time any more. When viewing the flow down from a roof via a rainspout, it is probable that most of the potential energy is lost due to turbulence. Based on this assumption, all cell slope values of over a hundred percent were cut to twenty percent (see Figure 24), a rough approximation of average roof slope, using the *Raster Calculator* tool (Esri, 2012).

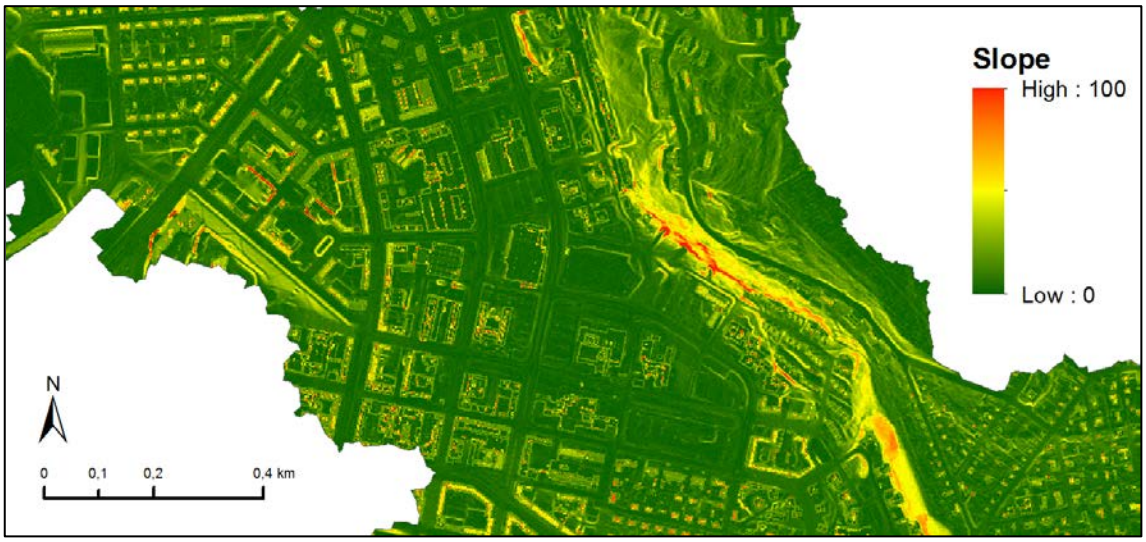

Figure 24. Slope raster with all building-related slopes of over 100 % cut down to 20 %.

In the SWMM conceptualization, flow paths from upstream cells to pour points are straight parallel lines. In reality, these lines lie superimposed in the stream cells. Thus, to get results consistent with the SWMM conceptualization, the areal mean slope had to be weighted by the flow rate at each cell. This was achieved by first multiplying the slope raster with the flow accumulation raster. As the slope parameter should characterize only overland flow, the cells where flow happened in stormwater drains had been set null in the FAC before the multiplication. A subcatchment-specific zonal sum was then calculated with the *Zonal Statistics* tool (Esri, 2012) both for the multiplication result raster (*zonal sum A*) and the modified FAC (*zonal sum B*). The final flow-weighted slopes for all subcatchments were obtained by dividing *zonal sum A*:s with *zonal sum B*:s. These areal slopes are presented in Figure 25 and further discussed in Chapter 5.2.8.

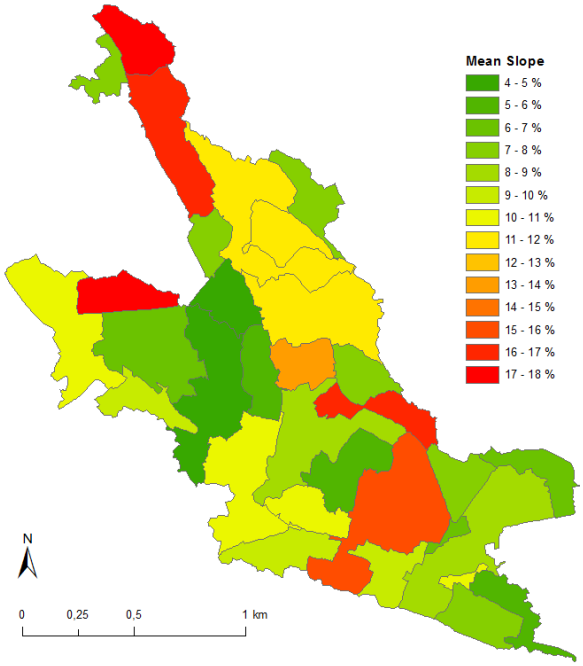

Figure 25. Subcatchment mean hydrologic slopes that were used as model parameters.

5.2.5. Manning's roughness coefficient *n* for overland flow

For impervious areas the roughness coefficient *n* was set to the value of 0.011, which is the literature value for smooth asphalt (Rossman, 2010). For non-asphalt surfaces, this was considered a good compromise between smoother materials (e.g. rooftops), and slightly rougher materials (e.g. concrete).

For pervious areas an *n* value of 0.3 was used. This was a compromise between the values for short grass (0.15), dense grass (0.24) and woods with light underbrush (0.40) (Rossman, 2010).

5.2.6. Flow width

Flow width is one of the least tangible SWMM parameters. It is defined as the '*characteristic width of the overland flow path for sheet flow runoff*' (Rossman, 2010).

Very typically it is used as a calibration parameter (Park et al., 2008; Gironás et al., 2009), although there are ways to deduce an initial estimate even without calibration. According to Rossman (2010) and Gironás et al. (2009), the width parameter can be calculated by dividing the subcatchment area by the length of the longest overland flow path in the area. In case several flow paths exist, their maximum lengths should be averaged. Channelized flow should never be included in this flow length, which typically reduces the maximum flow length to less than 200 meters; on urban areas even below that (Gironás et al., 2009).

As calibration was not possible in this study, an appropriate width estimate had to be calculated. The subcatchment areas being well known, this was merely a question of defining appropriate flow lengths. A good aid in the calculations was the ArcGIS *Flow Length* tool (Esri, 2012). It takes the FDG as an input and calculates for each cell the longest upstream (or downstream) flow route.

First, the downstream flow length before channelizing was obtained for all cells of the FDG by running the *Flow Length* tool (Esri, 2012) with an upstream setting. A weight raster was also defined to prevent stream cells being counted as additional overland flow length. The weight raster had been created by setting all the pipe cells in the drainage network raster to zero, and all other cells as one.

Next, all the upstream source cells within the subcatchments were identified by running the *Flow Length* tool (Esri, 2012) with an upstream setting. All the cells in the resulting raster with an upstream flow length of zero were interpreted as source cells. A new raster was then created, and its values were set by Raster Calculator according to the following principles: (i) if the cell was a source cell, its value was set to the downstream flow length, and (ii) all other cells were set null.

Last, the results had to be summarized for each subcatchment. The first approach was using the *Zonal Statistics as Table* tool (Esri, 2012). The subcatchment flow length appeared to be 62 m on average, with individual values ranging from 19 to 240 m. An interesting remark was that source cells accounted on average for 29 % of the subcatchment area (varying from 19 % to 36 % for individual subcatchments).

The above number of source cells did sound rather high, as in the SWMM conceptual model source cells would only occupy one row of cells at the upstream edge of the rectangular subcatchment. Then, theoretically, the portion of source cells of the subcatchment area should be:

$$(W_F L_C)/(W_F L_F) = L_C/L_F \ , \tag{17}$$

where
W_F = flow width parameter (m),
L_F = flow length parameter (m),
L_C = raster cell size (m).

Thus, if the flow length was 62 m, the source cells should cover only 3 % of the subcatchment area and not 29 % like in the above average.

To test how fulfilling the above equation would affect the flow length, the raster of the source cell downstream flow lengths was converted into point features and imported into Excel. The idea was to select only a certain share of the highest cell flow lengths so that the above equation would be true. Through manual iterations on several subcatchments it was found that counting only the highest percentile of the flow lengths on each subcatchment would fit the equation reasonably well.

The final approach resulted in source cells to account only for 0.3 % of the subcatchment area, on average. Correspondingly, the mean flow length was 210 m, with values ranging from 77 to 449 m (see Figure 26). On average, flow lengths were 3.8 times greater than those of the first approach.

Flow widths were finally calculated by dividing the subcatchment areas by the flow lengths acquired through both of the above approaches. Results for the approach B are presented in Figure 26 below.

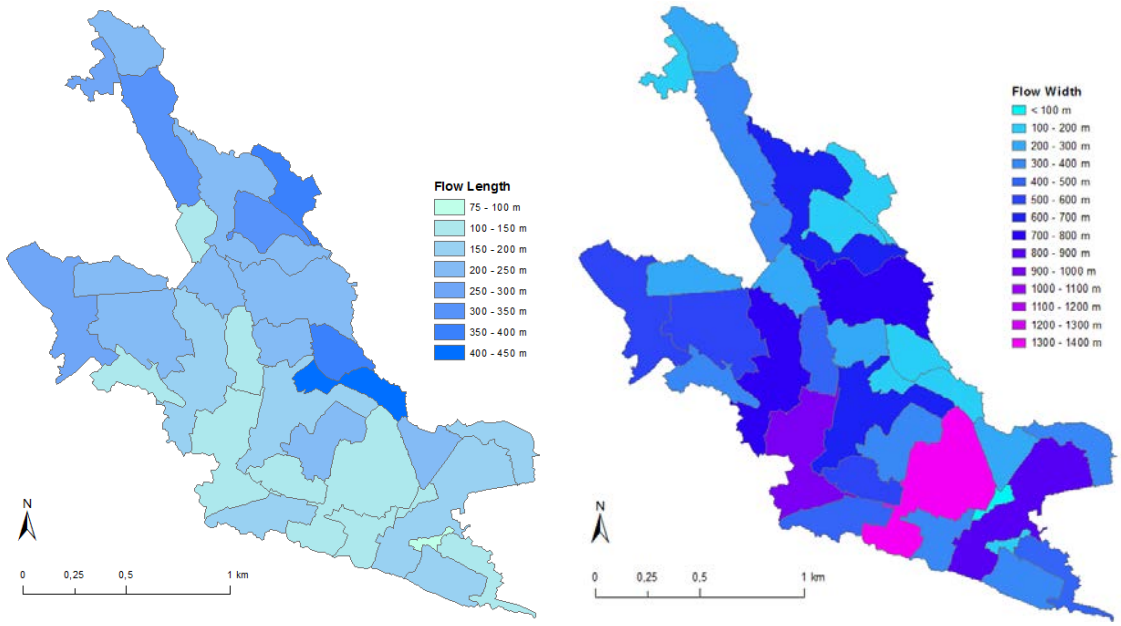

Figure 26. Subcatchment flow lengths (left) and flow widths (right) obtained using the approach B.

The results were compared with the results by Krebs (2013) who has made parameter calibrations in two of the subcatchments in question.

5.2.7. Snowpack accumulation and snowmelt

The form of precipitation and snowmelt processes were modeled based on air temperature data. There are three different types of snow pack objects in the model: (i) plowable area, (ii) impervious area, and (iii) pervious area. For each of these, the following parameters had to be defined (Rossman, 2010):

- minimum and maximum snow melt coefficients,

- threshold air temperature for snow melt to occur,
- snow depth above which 100 % areal coverage occurs,
- initial snow depth,
- initial and maximum free water content in the pack.

First, the snowmelt parameters were set as follows:

- threshold temperature for dividing precipitation between snowfall and rain = 2 °C (Dingman, 1994),
- antecedent temperature index (ATI) weight = 0.5 (Rossman, 2010),
- negative melt ratio = 0.6 (Rossman, 2010),
- elevation above mean sea level = 85 m (a rough average based on DEM),
- latitude = 60.989 °N,
- longitude correction = 0 min.

Next, a snowpack object was created and parameterized. SWMM calculates the snowmelt based on hourly melt coefficients. For Finland, only degree-day melt coefficients were available (e.g. Kuusisto, 1986b). Hourly values could not be computed from daily values as the relation between the daily and hourly coefficients is not linear. The best reference was given by Valeo and Ho (2004), who present some calibrated hourly melt coefficients for a catchment in Calgary, Alberta, Canada. Due to an approximately ten-degree difference in latitude, values needed to be slightly reduced to account for the decreased solar radiation when applied in Lahti. The minimum values (for December 21st) were cut by 3 %, and the maximum values (for June 21st) by 25 %.

Based on the snow depth measurements, the initial snow depth and the initial free water in the snowpack were both set to the value of 0 mm. Free water holding capacity as a fraction of snowpack depth was set to 0.20 which is a compromised value suitable for shallow packs both in early winter and spring (Huber et al., 1988). Snow melt base temperature was set to 0 °C. A small correction could have been appropriate here due to the microclimatic difference between the weather station and the study area (see Chapter 4.2.3). Such was still not done to maintain comparability of the modeled snow depth with the snow depth measurements at the same weather station. Last, the snow depth above which there is 100% cover was defined to be 10 mm water equivalent (Ho, 2002).

No data on plowing and snow removal were available. The fraction of the plowable area was thus set to zero. If there had been any data, snow plowing regimes could have been accounted for in the simulation.

5.2.8. Summary of subcatchment parameterization

This study showed that subcatchments can be rapidly parameterized by combining GIS methods with literature values. The parameterization process and results are briefly assessed here. Most of the parameters used in the model are presented in Table 4 to give

an overall view on the results of the parameterization. The table also presents comparison with the parameter values by Krebs et al. (2013a; 2013b) who performed a high-resolution parameterization for a detailed surface discretization and then aggregated the parameters to single catchments. They also conducted a calibration for these lumped catchments.

Table 4. Comparison of parameter values with Krebs et al. (2013a; 2013b).

Parameter	Source	Subcatchment "TP"		Subcatchment "AP"		Mean difference to weighted average
		This study	Weighted average by Krebs et al. (2013a; 2013b)	This study	Weighted average by Krebs et al. (2013a; 2013b)	
Area [ha]	GIS methods	5.69	5.85	5.26	7.00	- 14 %
Imperviousness [%]	GIS methods	96.1	85.8	74.8	53.7	+ 26 %
Slope [%]	GIS methods	4.30	5.17	10.0	14.4	- 24 %
Flow width [m]	GIS methods	256	168	502	350	+ 48 %
Flow length [m]	GIS methods	222	349	105	200	- 42 %
Depression storage (impervious) [mm]	Literature	1.9	0.45	1.9	0.51	+ 297 %
Depression storage (pervious) [mm]	Literature	5.1	4.1	5.1	3.4	+ 37 %
Manning's n for impervious areas [-]	Literature	0.011	0.021	0.011	0.014	- 35 %
Manning's n for pervious areas [-]	Literature	0.3	0.161	0.3	0.275	+ 48 %

As discussed in Chapter 5.1.5, the DEM-based subcatchment delineation was considered to be successful. The inaccuracy in the subcatchment areas was largely explained by the different locations of the subcatchment pour points. Differences in other parameters, too, were partly induced by averaging the parameters over different geographical areas. Other possible reasons for the difference are discussed in the following paragraphs.

Imperviousness percentages calculated from the High Density Imperviousness Layer showed larger values than those of Krebs et al. (2013a; 2013b).This was believed to be due to some type of systematic error in the production of the HD Imperviousness Layer. The Europe-wide dataset was probably not capable of taking into account all the local factors such as differences in surface materials used in each geographical area. It could also be that not all of the total impervious area (TIA) indicated by the HD Imperviousness Layer actually behaved as effective impervious area (EIA). For SWMM parameterization, the difference could, if one wanted to, be compensated by calibration based on a few subcatchments of different land use types. Nevertheless, even with some additional calibration effort this method would have required only a moderate amount work. The method seemed thus highly promising for imperviousness parameterization of a large number of SWMM subcatchments. Another interesting subject would have been to experiment the above methodology with the new verified national Corine Land Cover 2012 imperviousness data, which unfortunately was not yet published at the time of this study (Finnish Environment Institute, 2013).

The slope of the overland flow was one of the parameters with values highly resembling the aggregated values by Krebs et al. (2013a; 2013b). The method of calculating slopes seemed to work at least for the two subcatchments where comparison was possible. The average slopes obtained are slightly lower than the calibrated values, probably indicating that the slopes for flow from roofs were reduced too much. Maybe the

majority of the potential energy is not being lost due to turbulence after all. The workflow for calculating subcatchment slopes had many steps. With the routine now established, it can though be performed more rapidly.

Flow width and flow length showed notable difference to the values by Krebs et al. (2013a; 2013b). This was no surprise. Like told above, flow width is one of the least physically-based SWMM parameters, typically used as a calibration parameter. The above-described method cannot be considered to be the best possible for calculating flow width. The method included some manual work, yet the results were not really applicable. An interesting remark is though that the flow lengths by Krebs et al. (2013a; 2013b) are higher than the maximum possible overland flow lengths suggested by Woolhiser (1981) or Gironás et al. (2009). The reason is that in a low-resolution modeling approach the flow length also needs to account for some parts of the otherwise ignored gutter or small-pipe flow in addition to the true overland flow. This explains the uncommonly high flow lengths.

For the flow width, it was challenging to find any physically-based aggregated values. Such aggregated approaches are in fact against the conceptual basis of the SWMM software. This study presented some attempts to do so, but the results are not very successful. The approach used poorly took into account the channelized overland flow which has not yet entered the drainage network. It would be probably preferable that flow width was kept as a calibration parameter, if possible.

For the literature-based parameters, the values adapted in this study clearly differed from the aggregated values by Krebs et al. (2013a; 2013b). It must be concluded that reliable aggregated values of depression storage and Manning's roughness coefficient cannot be directly drawn from literature.

Infiltration parameters are not repeated in Table 4 as there was no reference available. The national datasets used were not detailed enough as they had no coverage for urban areas. On the other hand, even detailed maps would not have helped because infiltration in urban areas may be more dependent on the compaction of the soil surface than the actual soil type.

Whether the above parameters provided realistic results in modeling shall be further discussed in Chapter 5.4.

5.3. Stormwater conveyance system parameterization

As described in Chapter 4.2.2, the stormwater system data was of poor quality, and the attributes had been stored inconveniently. Time-consuming pre-processing was thus inevitable to make the data suitable for stormwater modeling.

5.3.1. System links (conduits)

Visual inspection revealed that many of the pipe features had identical duplicates in the data. That was obviously incorrect. Hence, the features were dissolved so that the

duplicates with the exactly same location and attributes were eliminated. There is yet a small risk that some real parallel pipes were deleted in the process. However, any real parallel pipes had typically been stored at slightly different locations, resulting in none of them being lost.

The pipe diameters were only available as attributes of point features in the proximity of the pipes. The points also had one attribute telling the angle of the pipe in relation to North. This was first considered potentially helpful in automating the process of attributing diameters to pipes. However, a more practical routine was to use the *Join by Location* tool (Esri, 2012) to assign the attributes of nearby points to pipes. This was done for all points indicating a diameter of 500 mm or more. For a number of pipes, no nearby points were available. In all those cases, the diameters had to be interpolated manually based on the known upstream and downstream diameters. There were also some points indicating diameters of less than 500 mm even if the next upstream pipe section was 500 mm or more. Such contractions were not interpreted as errors as they can exist also in reality; especially on steep hillslopes where a smaller pipe will be capable of conveying the same discharge as the larger pipe at the top of the hill.

The parameterized pipe network had to reach all the pour points of the subcatchments. As noted in Chapter 5.1, the 500 mm pipes did not always reach far enough upstream. For some subcatchments, the pipe network had to be extended by manually defining diameters for some pipes smaller than 500 mm. On the contrary, in other subcatchments the 500 mm pipes reached further upstream than to the pour point. The excess pipes were trimmed by manual editing.

At this point, the network in study area B consisted of nearly thousand pipe features. To maintain simplicity, consecutive pipe features of the same diameter were dissolved into one with the *Dissolve* tool (Esri, 2012), with the option ‘Unsplit Lines’ set as false. The number of resulting features was 52. Some of these features were continuous even over locations where there should have been a junction with another pipe. The *Feature Vertices to Points* tool (Esri, 2012) with the option ‘Both Ends’ was used to create a set of points at the ends of the pipe sections. Duplicate points were deleted with the *Delete Identical* tool (Esri, 2012), resulting in a point dataset including all the junctions (and inlets/outfalls) needed for modeling. Pipe features were then split at all junctions using the *Split Line at Point* tool (Esri, 2012). In the end there were 58 pipe features in the data (see Figure 27).

It must be noted that the above described dissolving technique reduces the accuracy of the model. Some manholes and lesser pipe junctions were ignored if the incoming and outgoing pipes were of the same diameter. As a result, the pipe slopes were averaged, always assuming a constant slope between two major junctions.

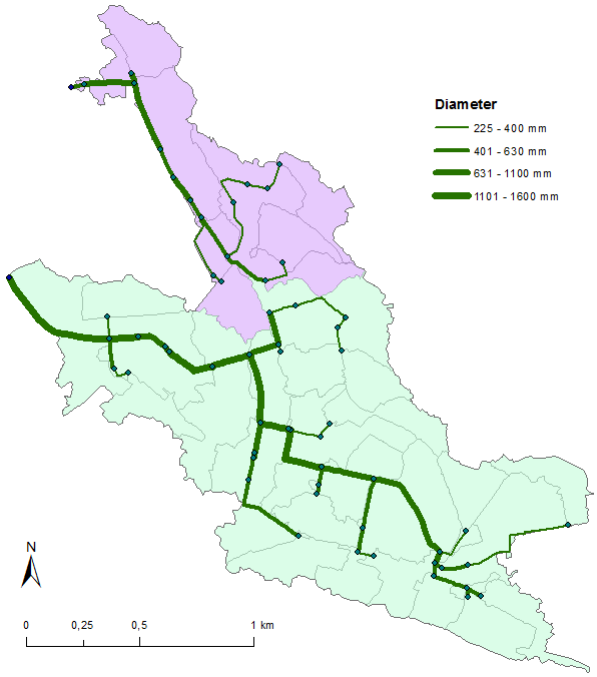

Figure 27. Stormwater drainage network used in modeling. System nodes are shown as dots and system links as green lines of a varying thickness representing the pipe diameter.

Pipe length and the pipe end elevations are necessary parameters for hydraulic modeling in SWMM. Lengths were obtained as ArcGIS geodatabase format has a standard field indicating the length of the feature. Elevations needed more work, as those were presented in the data as attributes of separate points which were geometrically connected to the pipe ends by another layer of polyline features. Attempt was first made to develop an automatic procedure. The complexity of the data structure unfortunately prevented most approaches to correctly join the elevation points to the pipes and thus transfer the attributes. For a larger study area developing such a method could have been feasible, although probably not of any general use on other sites. Another option could have been using the *Interpolate Shape* tool (Esri, 2012) to approximate the pipe slopes based on the DEM but the results would inevitably have been inaccurate. Hence, the most feasible option was to label the points with the attributes and manually attribute the elevations to the pipes. There were anyway only 58 pipe features in the data. This routine worked well but would not have suited very well for an area any larger. In addition, there was a definite risk of humane error in manually typing over a hundred elevation records.

After pipe lengths and elevations were determined, the Manning's roughness coefficient *n* had to be defined. No data was available on the pipe materials in the study area. Typically in Finland, most of the sewer pipes (over 70 %) are made out of plastic, concrete being the second most common option (24 %) (FCG Planeko Oy, 2008). According to the SWMM User's Manual (Rossman, 2010), *n* value of 0.011 to 0.015 applies to both of these materials. Many of the pipes in the city center area are relatively old, and thus probably not as smooth as new pipes. Thus, roughness coefficient of 0.015 was used for all pipes.

5.3.2. System nodes (inlets, manholes, etc.)

The point feature class containing all the junctions, inlets, and outfalls was created by the *Feature Vertices to Points* tool (Esri, 2012) as described above. Overall, 62 points were included. The two outfalls were first moved to a new feature class. Each of the remaining points had to be then given attributes for invert elevation and maximum depth. Invert elevation tells the elevation of the bottom of the manhole (in the N2000 reference system). As no data on this was available, the elevation was set by hand at 10 cm below the level of the lowest pipe connected to the manhole.

Maximum depth tells the elevation difference between the manhole invert and the ground surface. *Add Surface Information* tool (Esri, 2012) was used to add to the points a new field for ground level based on the DEM. Maximum depth could then be computed by subtracting the invert elevation from the ground level.

For the two outfall points, invert elevations were set at the elevation of the incoming pipe ends. As both outfalls are below the water level of Lake Vesijärvi, a fixed type boundary condition with the water elevation at the mean water level of N2000+81.4 meters was appropriate.

5.3.3. Summary of stormwater system parameterization

Parameterization of the transport compartment of SWMM was straightforward. However, work load was unnecessarily increased by the problematic structure of the input data (see Chapter 4.2.2). More detailed input data could considerably reduce the work needed here, thus enabling the inclusion of a less-skeletonized high-detail drainage network in the SWMM application. Such data might also prove valuable in the catchment delineation and subdivision process, as e.g. the allocation of pour points could be based on an increased amount of pipe information. In addition, this would also allow for a higher degree of detail for the catchment surface discretization. If large areas were to be modeled, input data of a consistent structure with detailed attributes would be a necessity to maintain feasibility.

The non-random selection of the study area resulted in a drainage system less complex than what could have been the case in an arbitrarily chosen area. There were no notable natural streams in the study area, and all the stormwater was drained via separate sewers. The need to model combined sewers or open channels would have increased the complexity of the model and, accordingly, the challenge experienced.

If concentrating on the long-term water balance like in the example simulations of this study, the impact of the drainage system is of minor importance. The structure and parameters of the drainage network grow important only when modeling single runoff events, trying to estimate peak flows, for example. Calibrating the transport system model would in such a case be highly necessary as the way of using literature values like in this study seems to be generalizing. In addition, the methodology of this study led to only a partial reproduction of the hydraulic properties of the drainage network.

The manholes along a pipeline with a constant diameter were for example omitted through the dissolving of the pipe data. Neither were possible stormwater pumping stations in the study area modeled, as no data about their operation was available.

One major cause of uncertainty is the fact that the smallest pipes were not being modeled at all. Practically, the modeled flow 'jumps' from the sewer inlets straight into the main sewers. This discontinuity should have been taken into account in the flow width calculations. Another option might have been to create some kind of imaginary conduit between the center point of each subcatchment and the pour point related.

5.4. SWMM simulations

To put the above subcatchment and conveyance system parameterization to the test, selected model runs were performed and their results analyzed. In the absence of adequate runoff measurements, no actual validation of the model could be made. Hence, the emphasis was on 'sanity checking' the results against literature and the snow depth measurements.

The actual SWMM model was developed from the ArcGIS data. All the features parameterized above had been stored in four separate Esri Shapefiles (subcatchments, junctions, conduits, and outfalls). For modeling, the geometry and attributes of all features were then converted into a SWMM project file using a custom-made Perl script. This worked well and the model created was usable right away (see Figure 28).

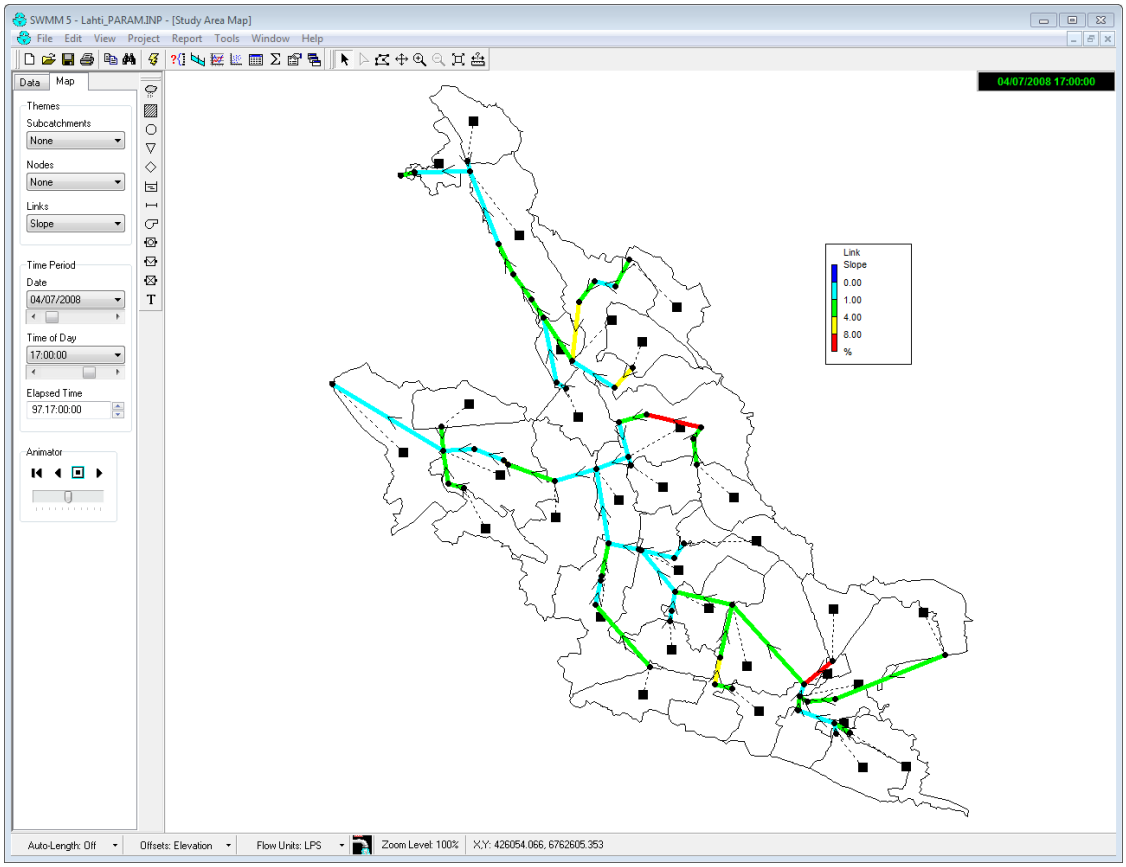

Figure 28. Structure of the SWMM model. Flow direction in the conduits is presented by arrows.

Before aiming for any actual results from the model, proper simulation time steps were to be chosen. The reporting time step and the dry-weather hydrologic time step were set to one hour. The hydraulic routing time step was set to 30 s, which was expected to be sufficiently short for dynamic wave routing (Rossman, 2010). The wet-weather time step was also set to 30 s.

The model was run with hourly precipitation data for the entire time period covered by the weather observations, from 1 Jan 2008 until 21 Nov 2011 (later referred to as the 'long-term simulation'). Additional model runs were performed individually for each year during that period. Also, some shorter periods were modeled to compare the model performance between winter and summer conditions.

Careful inspection of the modeling results showed that there was a software error in the way SWMM computed infiltration during winter conditions. All precipitation falling on pervious surfaces in the form of snow was counted twice in the modeling results. The water both remained in the form of snow, and at the same time was falsely counted as infiltration. On some subcatchments, this resulted in long-term infiltration sums exceeding the total precipitation. The same error has been reported also by Dickinson (2012), who states the error is going to be fixed in the next SWMM model build (version 5.0.023). Before further analysis, all the results concerning water balance needed therefore to be corrected by reducing the sum of snowfall on pervious areas from the sum of infiltration on the same areas. This correction was performed in spreadsheet software.

Preliminary results for the long-term water balance showed that practically no runoff was generated on the pervious parts of the catchments due to excessive infiltration. This is probably due to uncertainties in the selection of infiltration parameters. The real soil type might not be sandy loam but silt loam, for example. Also, the actual value of maximum initial moisture deficit may be reduced due to groundwater interaction.

5.4.1. Modeled vs. measured snowpack accumulation and snowmelt

When modeling snowpack accumulation and snowmelt, the wet-weather time step was increased to 1 h. The model was run for the period of nearly four years starting in the beginning of 2008, and the resulting snow water equivalent was plotted against snow depth measurements from Lahti-Laune (Figure 29). Through visual inspection of the graphs it becomes evident that the model results closely resemble the measurements.

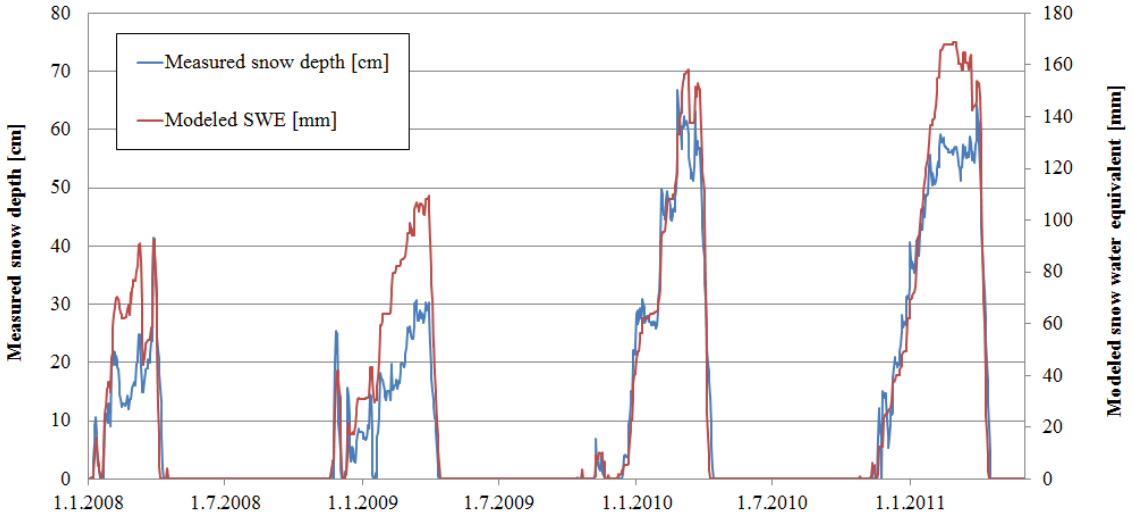

Figure 29. Modeled snow water equivalent versus measured snow depth.

Nevertheless, snow depth should not be directly compared with the snow water equivalent. Their mutual proportion, the bulk snow density, is not constant but varies over time, typically growing along the snow season and being highest just before the snow melts away. The bulk snow density was calculated here by dividing the *modeled* snow water equivalent by the *measured* snow depth. The result is plotted in Figure 30.

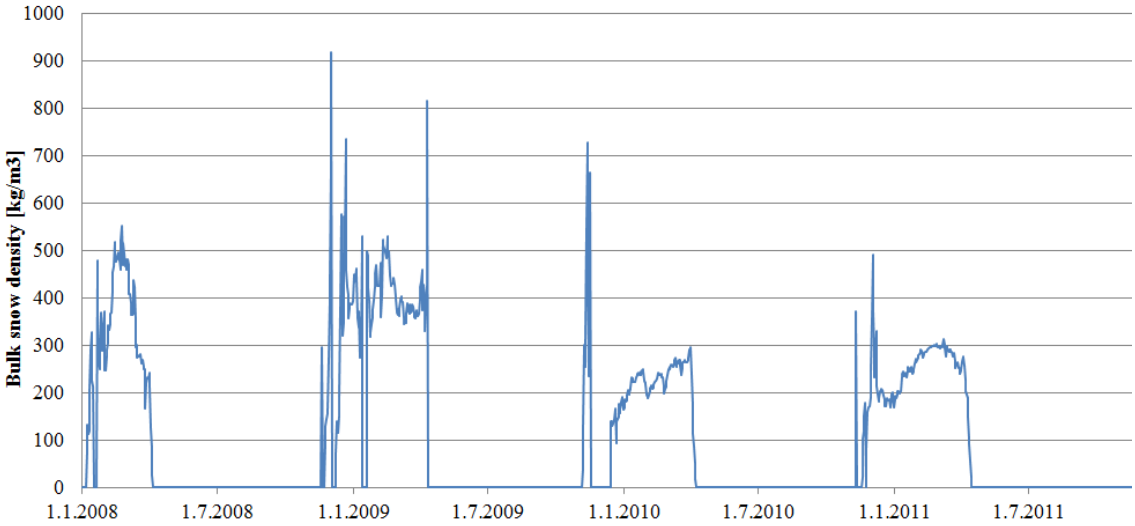

Figure 30. Bulk snow density calculated as a relation of modeled SWE and measured snow depth. The values have been calculated only for days with a minimum of 1 cm of measured snow depth.

The high peaks in Figure 30 are mostly values for days with only little measured snow on the ground, say, less than 3 cm. Such would be typical for slushy autumn and early winter conditions. The overall annual trend of the bulk snow density varies. For winters 2009–2010 and 2010–2011, the steady growth of bulk snow density from ca. 150 kg/m^3 at the time of Christmas to 300 kg/m^3 in the spring can be observed. This behavior well resembles the common understanding on the growth of bulk snow density through the snowy season (see Chapter 2.1.5). Of course, calibration would still yield better results.

It would though require measurements of snow water equivalent, not just the snow depth currently being measured near the study area.

5.4.2. The annual water balance

To study if the model could correctly reproduce the components of the annual water balance, the model was run separately for each year between 2008 and 2011, as well as for the whole time period at once. The modeled components of the annual regional water balance for the study area are presented in Table 5.

Table 5. Modeled annual and long-term water balance components for the study area B as a whole. The change of storage indicates the change in the amount of water stored in the snowpacks on the study area.

	2008		2009		2010		2011 (until 21.11.)		1.1.2008 - 21.11.2011	
	[mm]	in relation to precipitation	[mm]	in relation to precipitation	[mm]	in relation to precipitation	[mm]	in relation to precipitation	[mm]	in relation to precipitation
Precipitation	896	100 %	625	100 %	577	100 %	534	100 %	2632	100 %
Runoff	417	47 %	269	43 %	240	42 %	218	41 %	1172	45 %
Infiltration	353	39 %	256	41 %	186	32 %	167	31 %	952	36 %
Evaporation	95	11 %	78	12 %	79	14 %	92	17 %	344	13 %
Change of storage	31	3 %	18	3 %	21	4 %	-65	-12 %	5	0 %
Continuity error	1	0.1 %	5	0.8 %	50	9 %	122	23 %	165	6 %

Pervious areas sum up to a total of 45 % of the total study area B, meaning the maximum possible long-term infiltration should not exceed 45 % of the total precipitation. The modeled long-term infiltration is 36 % of the precipitation, thus fulfilling the above condition.

The modeled long-term runoff coefficient was 0.45, thus equaling the degree of imperviousness of the study area. For comparison, Kotola and Nurminen (2003) measured a slightly lower average runoff coefficient of 0.29 for non-winter conditions on another urban catchment (Vallikallio; 50 % impervious land cover), in the city of Espoo in southern Finland.

The continuity error seems to be induced by annual snowfall, indicating there might still be an error in the method of correcting the false infiltration related to snowfall (see further discussion in Chapter 5.4.3). For years with small measured snow depths (2008 and 2009) the continuity error was clearly smaller than for the more snowy years (2010 and 2011). The model was run once also for the summer season of 2010, resulting in a continuity error of only 0.001 %. This is a sign that the error would be caused during modeling the snow processes as was expected. More research on this was still needed.

5.4.3. Uncertainties related to the selection of time steps

The impact of the wet-weather modeling time step on the long-term water balance was studied by varying the time step between long-term simulations otherwise identical. Lengthening the time step in the range of 10 seconds to 1 hour resulted in a growing continuity error caused by a faulty decline in infiltration. With a wet-weather time step of 30 s the continuity error for runoff was still at a rather tolerable level below 10 %, but with time steps of several minutes the error rapidly increased to over 15 %.

Furthermore, modifying the wet-weather time step was also found to have a large impact on snow water equivalent (SWE) and snowmelt. The model was run for a four-month time period from January 2008 through April 2008 with several different wet-weather time steps. For winter conditions, a short wet-weather time step (roughly 30 s or less) yielded an acceptable continuity error, but very little snow was accumulated (see Figure 31). A longer wet time step of 5 min resulted in larger snow accumulation, but at the same time continuity errors exceeding 20 %.

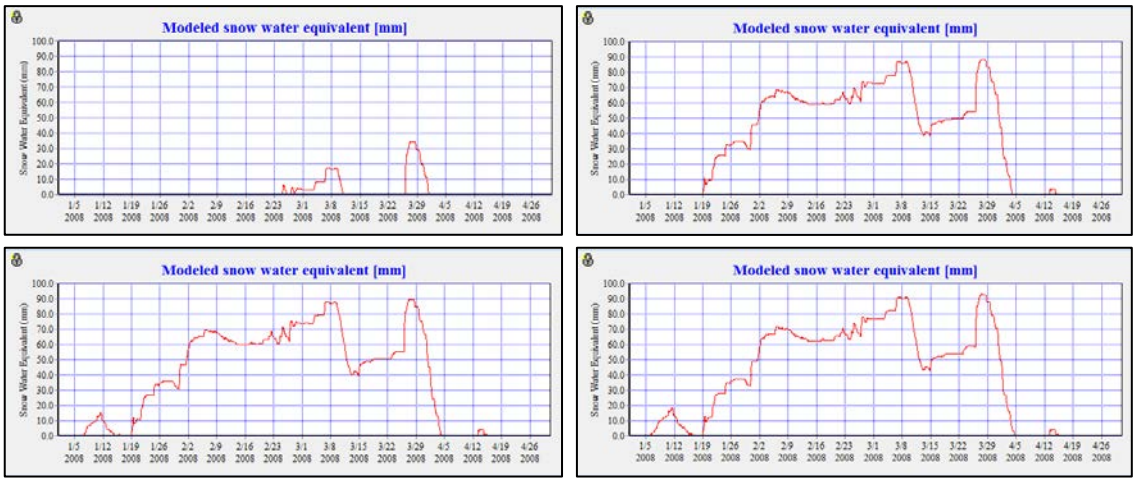

Figure 31. Modeled SWE during Spring 2008 using a wet-weather time step of 30 s (upper left), 1 min (upper right), 5 min (lower left), and 1 h (lower right).

While using the 1-hour wet-weather time step, the model seems to produce reasonable-looking dynamics of modeled snow-water equivalent. Further lengthening of the time step would not probably have added to the snowpack notably. On the other hand, a much shorter time step would have resulted in obviously too low amounts of snow on the ground, as discussed above.

To conclude, choosing for appropriate simulation time steps is not straightforward. No such wet-weather time step for a long-term simulation could be found that the snowpack accumulation would have been realistic while the continuity error remained small. A one-hour wet-weather time step had been used when examining snow accumulation, whereas for long-term water-balance calculations the time step had been set to 30 seconds. The latter resulted in a long-term continuity error of 7 %.

For the reasons stated here, the water-balance results in Chapter 5.4.2 using a short 30-second wet-weather time step are probably though not fully realistic. The short step appears to lead to very limited snowpack accumulation and surface runoff is thus experienced through the whole winter season. This could result in too much infiltration on an annual level.

5.4.4. Summary of SWMM simulations

The SWMM simulations performed to test the reasonability of the model were disturbed by excessive runoff continuity error. The error was evidently attributed to the snowpack accumulation and snowmelt processes. Partly the error was caused by a publicly known

flaw in the model algorithm, which could be quite simply counteracted by numerically altering the water balance results. However, for some reason this correction did not completely remove the snow-related continuity error. Maybe the logic of the correction method used was somehow faulty, or maybe there is also some other mechanism increasing the continuity error for long-term snow process simulations. Either way, the behavior of the modeled water-balance components could not be properly assessed. The results suggest that there may be some error regarding the snow processes in the current SWMM version.

The 1-hour simulation results for snow water equivalent showed good accuracy compared to the measured snow depths. A thorough comparison was not possible as the snow water content relating the two properties was unknown. These simulations were solely based on literature values, indicating that reasonable results for snow processes may be obtained with SWMM even without model calibration.

6. CONCLUSIONS

The overall objective of this study was to identify a catchment delineation and parameterization that support an application of SWMM (Stormwater Management Model) in a large urban area.

Detailed catchment delineation and subdivision was successfully performed in two urban catchments with a total area of 2.64 km^2. This resulted in 32 subcatchments with an average area of 8.2 hectares. The process involved substantial manual work but can henceforth be sped up by the routines established in this study. A complete automation would however be impossible due to the typical defects in input data. The results showed sufficient spatial accuracy for the intended use. Altogether, a catchment delineation and subdivision for use in SWMM modeling was found feasible to perform even for a large urban area using a GIS-based approach. Publicly available spatial data and data on stormwater system layout are all that is needed as process input.

Parameterization of heterogeneous subcatchments of low spatial resolution turned out to be challenging and inaccurate. No clear procedures have been presented in literature on how to choose certain parameter values in an aggregated SWMM approach without calibration. A combination of GIS methods and literature values was used for the purpose, but the results were found partly inaccurate with respect to calibrated values. To reliably use the results in modeling, either calibration should be performed or the model sensitivity for the most hard-to-define parameters such as flow width or depression storage should be proved minor.

The effort needed for drainage network parameterization proved to be highly dependent on the quality of the input data. If the pipe and junction data has many gaps or is stored in the database in a cumbersome manner, detailed modeling of large systems may easily grow non-feasible.

The SWMM model runs conducted were troubled with excessive continuity errors. This is a sign that the selection of appropriate simulation time-steps for long-term modeling with low spatial resolution is not simple and should be further studied. Continuity errors cause the results for urban water balance to be slightly biased.

Overall, the methods developed in this study provide a feasible approach for SWMM parameterization for large urban areas. Despite the further research still needed, non-calibrated SWMM applications of low spatial resolution seem promising for certain tasks in stormwater modeling. The approach would suit especially for rapid stormwater modeling when studying large-scale processes, such as the effects of the climate change on urban water balance.

Suggested future studies

There are several lines of research that ought to be further worked upon based on the findings of this study. The above discussed results seem to provoke a great number of

related questions to which the answers could be found by conducting more simulations with the model built for this study.

Regarding subcatchment delineation for use in SWMM modeling, the best method of choosing pour points to get catchments subdivided to a certain degree should be sought for. These methods could also be developed to aim for land-use homogeneity within the subcatchments. Related to that, the general effect of the subdivision level on the model performance would be useful to explore. It could definitely be worth trying to experiment with an even finer subdivision scheme if only drainage network data of a better quality was available.

One of the major problems to be solved is finding out whether the continuity errors observed could be reduced by a careful selection of simulation time-steps. Here, some experiments were already made regarding the wet-weather time step but the results were poor. It would be interesting to know, whether also the dry-weather time step could affect the errors. What might also be useful is to judge if the most appropriate time steps are different for winter and summer conditions, as the results here suggest.

Moreover, it would be interesting to study the outcome of using weather observations data of different time-resolutions. It may be that the partly-hourly-partly-daily data used here was not accurate enough for the task at hand.

Further analysis should also address in more detail the precision of the long-term water balance components given by the simulations. If those results were found to be far from reality, it would be valuable to see how the methods proposed here could be refined for a better outcome. Proving the results on water balance components well-reasoned would also open possibilities to use coarse-scale long-term SWMM modeling for simulating the effect of climate change scenarios in large urban areas.

Finally, with any research based on a non-calibrated model, parameter sensitivity analysis would be of major importance. Here many parameters were only based on some general literature values. It would be of value to know how the inaccuracy of such values affects the reliability of the results. Further, changes of parameter impacts depending on the properties of the subcatchments would be interesting to look into.

REFERENCES

AALTONEN, J., HOHTI, H., JYLHÄ, K., KARVONEN, T., KILPELÄINEN, T., KOISTINEN, J., KOTRO, J., KUITUNEN, T., OLLILA, M., PARVIO, A., PULKKINEN, S., SILANDER, J., TIIHONEN, T., TUOMENVIRTA, H. and VAJDA, A., 2008. *Rankkasateet ja taajamatulvat (RATU) - Suomen ympäristö 31/2008.* Vammala: Finnish Environment Institute (SYKE).

AMAGUCHI, H., KAWAMURA, A., OLSSON, J. and TAKASAKI, T., 2012. Development and testing of a distributed urban storm runoff event model with a vector-based catchment delineation. *Journal of Hydrology*, **420**, pp. 205-215.

BÄHR, H. and VÖGTLE, T., eds, 1999. *GIS in environmental monitoring.* Stuttgart: E. Schweizerbart'sche Verlagsbuchhandlung (Nägele u. Obermiller).

BARCO, J., WONG, K.M. and STENSTROM, M.K., 2008. Automatic calibration of the US EPA SWMM model for a large urban catchment. *Journal of Hydraulic Engineering*, **134**(4), pp. 466-474.

BELING, F., GARCIA, J., PAIVA, E., BASTOS, G. and PAIVA, J., 2011. Analysis of the SWMM Model Parameters for Runoff Evaluation in Periurban Basins from Southern Brazil, *12nd international conference on urban drainage* 2011, pp. 11-16.

BERNARD, J.M. and TUTTLE, R.W., 1998. Stream Corridor Restoration: Principles, Processes, and Practices, *Engineering Approaches to Ecosystem Restoration* 1998, ASCE, pp. 320-325.

CALLOW, J.N., VAN NIEL, K.P. and BOGGS, G.S., 2007. How does modifying a DEM to reflect known hydrology affect subsequent terrain analysis? *Journal of Hydrology*, **332**(1–2), pp. 30-39.

CANTONE, J. and SCHMIDT, A., 2011. Improved understanding and prediction of the hydrologic response of highly urbanized catchments through development of the Illinois Urban Hydrologic Model. *Water Resources Research*, **47**(8),.

CHEN, M. and TUCKER, C., 2003. *Comparing Different Approaches Of Catchment Delineation.* Citeseer.

CHOI, K. and BALL, J.E., 2002. Parameter estimation for urban runoff modelling. *Urban Water*, **4**(1), pp. 31-41.

DI GREGORIO, A., ed, 2005. *Land Cover Classification System: Classification Concepts and User Manual: LCCS.* Food & Agriculture Organization.

DICKINSON, R., 07/30/2012, 2012-last update, SWMM 5 or 5.0 Blog, InfoSWMM, InfoSewer [Homepage of Dickinson, R.], [Online]. Available: http://www.swmm5.net/2012_07_01_archive.html [06/19, 2013].

DINGMAN, S.L., 1994. *Physical hydrology.* Prentice Hall Upper Saddle River, NJ.

DISKIN, M.H., 1981. Nonlinear Hydrologic Models, V.P. SINGH, ed. In: *Rainfall-Runoff Relationship,* May 18-21 1981, Water Resources Publications, pp. 127--146.

DUNNE, T., 1978. Field studies of hillslope flow processes. *Hillslope hydrology*, **227**, pp. 293.

DURRANS, S.R., 2003. *Stormwater Conveyance Modeling and Design.* Waterbury, CT: Haestad Methods, Inc.

ESRI, 2012. *ArcGIS 10.1.* Redlands, CA, USA: Esri Inc.

FAIRFIELD, J. and LEYMARIE, P., 1991. Drainage networks from grid digital elevation models. *Water Resources Research,* **27**(5), pp. 709-717.

FCG PLANEKO OY, 2008. *Vesihuoltoverkostojen nykytila ja saneeraustarve.* 2312-C9259. Maa- ja metsätalousministeriö.

FINNISH ENVIRONMENT INSTITUTE, 2013-last update, Maankäyttö- ja maanpeiteaineistojen tuottaminen CORINE Land Cover 2012 -hankkeessa [Homepage of Finnish Environment Institute], [Online]. Available: http://www.syke.fi/fi-FI/Tutkimus__kehittaminen/Tutkimus_ja_kehittamishankkeet/Hankkeet/Maankaytto_ja_maanpeiteaineistojen_tuottaminen_CORINE_Land_Cover_2012_hankkeessa [06/06, 2013].

FINNISH METEOROLOGICAL INSTITUTE, 2013-last update, Ilmatieteen laitoksen havaintoasemat [Homepage of Finnish Meteorological Institute], [Online]. Available: http://ilmatieteenlaitos.fi/havaintoasemat [04/15, 2013].

FINNISH METEOROLOGICAL INSTITUTE, December 31, 2008, 2008-last update, Vuosi 2008 oli lämmin ja sateinen [Homepage of Finnish Meteorological Institute], [Online]. Available: http://ilmatieteenlaitos.fi/tiedote/1230711770 [05/08, 2013].

FLETCHER, T., ANDRIEU, H. and HAMEL, P., 2012. Understanding, management and modelling of urban hydrology and its consequences for receiving waters; a state of the art. *Advances in Water Resources,* .

GEOLAND2, 2010. *Technical note on HR imperviousness layer product specification.* geoland2 consortium.

GEOLAND2, 2009. *User Interface dossier - User requirements.* geoland2 consortium.

GEOLOGICAL SURVEY OF FINLAND, 2013-last update, Suomen maaperä 1:20 000 [Homepage of Geological Survey of Finland], [Online]. Available: http://fi.gtk.fi/tietopalvelut/geologiset/kartta_aineistot/ [02/15, 2013].

GHOSH, I., 2010. Characterizing and understanding the effects of spatial resolution in urban hydrologic simulations.

GHOSH, I. and HELLWEGER, F.L., 2011. Effects of spatial resolution in urban hydrologic simulations. *Journal of Hydrologic Engineering,* **17**(1), pp. 129-137.

GIRONÁS, J., ROESNER, L.A. and DAVIS, J., 2009. *Storm Water Management Model Applications Manual.* EPA/600/R-09/077. Cincinnati, Ohio: United States Environmental Protection Agency.

GÖBEL, P., DIERKES, C. and COLDEWEY, W.G., 2007. Storm water runoff concentration matrix for urban areas. *Journal of contaminant hydrology,* **91**(1–2), pp. 26-42.

GREEN, W.H. and AMPT, G., 1911. Studies on soil physics, 1. The flow of air and water through soils. *J.Agric.Sci,* **4**(1), pp. 1-24.

HAASE, D., 2009. Effects of urbanisation on the water balance – A long-term trajectory. *Environmental Impact Assessment Review,* **29**(4), pp. 211-219.

HAMILL, L., 2001. *Understanding Hydraulics.* Second Edition edn. Bristol: Palgrave.

HARGREAVES, G. and ALLEN, R., 2003. History and Evaluation of Hargreaves Evapotranspiration Equation. *Journal of Irrigation and Drainage Engineering,* **129**(1), pp. 53-63.

HO, C.L.I., 2002. *Urban snow hydrology and modelling.* Citeseer.

HORTON, R.E., 1933. The role of infiltration in the hydrologic cycle. *Transactions, American Geophysical Union,* **14**, pp. 446-460.

HUBER, W.C., DICKINSON, R.E., BARNWELL JR, T.O. and BRANCH, A., 1988. Storm Water Management Model, version 4. *Environmental Protection Agency,* **600**, pp. 3-88.

HYVÄRINEN, V. and PUUPPONEN, M., 1986. Valunta. In: S. MUSTONEN, ed, *Sovellettu hydrologia.* Mänttä: Vesiyhdistys ry, pp. 152-225.

JACOBSON, C.R., 2011. Identification and quantification of the hydrological impacts of imperviousness in urban catchments: A review. *Journal of environmental management,* **92**(6), pp. 1438-1448.

JANG, S., CHO, M., YOON, J., YOON, Y., KIM, S., KIM, G., KIM, L. and AKSOY, H., 2007. Using SWMM as a tool for hydrologic impact assessment. *Desalination,* **212**(1), pp. 344-356.

KABAT, P., HUTJES, R.W.A. and FEDDES, R.A., 1997. The scaling characteristics of soil parameters: From plot scale heterogeneity to subgrid parameterization. *Journal of Hydrology,* **190**(3–4), pp. 363-396.

KARVONEN, T. and KETTUNEN, J., 1986. Systeemianalyysi vesitaloudessa. In: S. MUSTONEN, ed, *Sovellettu hydrologia.* Mänttä: Vesiyhdistys ry, pp. 324-373.

KAUKORANTA, J., 2012. *Interview at Radio Voima, 04/22/2012.* Lahti: Radio Voima.

KERSALO, J. and PIRINEN, P., 2009. *Suomen maakuntien ilmasto.* 2009:8. Helsinki: Finnish Meteorological Institute.

KOTOLA, J. and NURMINEN, J., 2003. Kaupunkialueiden hydrologia–valunnan ja ainehuuhtouman muodostuminen rakennetuilla alueilla. *Teknillisen korkeakoulun julkaisuja,* **7**, pp. 80.

KREBS, G., KOKKONEN, T., VALTANEN, M., SETÄLÄ, H. and KOIVUSALO, H., 2013b. Spatial resolution considerations for urban hydrological modelling. *Journal of Hydrology (under review),* .

KREBS, G., KOKKONEN, T., VALTANEN, M., KOIVUSALO, H. and SETÄLÄ, H., 2013a. A high resolution application of a stormwater management model (SWMM) using genetic parameter optimization. *Urban Water Journal,* (ahead-of-print), pp. 1-17.

KUUSISTO, E., 1986b. Lumipeite ja jääilmiöt. In: S. MUSTONEN, ed, *Sovellettu hydrologia.* Mänttä: Vesiyhdistys ry, pp. 48-63.

KUUSISTO, E., 1986a. Sadanta. In: S. MUSTONEN, ed, *Sovellettu hydrologia.* Mänttä: Vesiyhdistys ry, pp. 29-47.

LAHDEN SEUDUN YMPÄRISTÖPALVELUT, 2010. *Lahden kaupungin hulevesiohjelma.* Lahti: Lahden seudun ympäristöpalvelut.

LIONG, S., CHAN, W. and LUM, L., 1991. Knowledge-based system for SWMM runoff component calibration. *Journal of Water Resources Planning and Management,* **117**(5), pp. 507-524.

MAUCHA, G., BÜTTNER, G. and KOSZTRA, B., 2011. European Validation of GMES FTS Soil Sealing Enhancement Data, L. HALOUNOVÁ, ed. In: *Remote Sensing and Geoinformation not only for Scientific Cooperation*, 05/30 - 06/02 2011, EARSeL, pp. 223--238.

MERZ, R. and BLÖSCHL, G., 2004. Regionalisation of catchment model parameters. *Journal of Hydrology,* **287**(1), pp. 95-123.

MONTZKA, C., CANTY, M., KUNKEL, R., MENZ, G. and WENDLAND, F., 2006. Remotely Sensed Land Cover and Impervious Surfaces Applied in Water Balance Modelling of a Mesoscale Catchment, *Proceedings of the 2nd Workshop of the EARSeL SIG on Land Use and Land Cover*, 09/28-09/30 2006, Center for Remote Sensing of Land Surfaces, pp. 307--314.

MUSTONEN, S., ed, 1986. *Sovellettu hydrologia.* Mänttä: Vesiyhdistys ry.

NATIONAL LAND SURVEY OF FINLAND, 2013d-last update, Maastotietokanta [Homepage of National land survey of Finland], [Online]. Available: http://www.maanmittauslaitos.fi/digituotteet/maastotietokanta [2/4, 2013].

NATIONAL LAND SURVEY OF FINLAND, 2013c-last update, Laserkeilausaineisto [Homepage of National land survey of Finland], [Online]. Available: http://www.maanmittauslaitos.fi/digituotteet/laserkeilausaineisto [2/4, 2013].

NATIONAL LAND SURVEY OF FINLAND, 2013b-last update, Korkeusmalli 2 m [Homepage of National land survey of Finland], [Online]. Available: http://www.maanmittauslaitos.fi/digituotteet/korkeusmalli-2-m [2/4, 2013].

NATIONAL LAND SURVEY OF FINLAND, 2013a-last update, Maanmittauslaitoksen ortokuva [Homepage of National land survey of Finland], [Online]. Available: http://www.maanmittauslaitos.fi/digituotteet/maanmittauslaitoksen-ortokuva [2/4, 2013].

NTELEKOS, A.A., SMITH, J.A., DONNER, L., FAST, J.D., GUSTAFSON, W.I., CHAPMAN, E.G. and KRAJEWSKI, W.F., 2009. The effects of aerosols on intense convective precipitation in the northeastern United States. *Quarterly Journal of the Royal Meteorological Society*, **135**(643), pp. 1367-1391.

PARK, S.Y., LEE, K.W., PARK, I.H. and HA, S.R., 2008. Effect of the aggregation level of surface runoff fields and sewer network for a SWMM simulation. *Desalination*, **226**(1–3), pp. 328-337.

RAWLS, W., AHUJA, L., BRAKENSIEK, D. and SHIRMOHAMMADI, A., 1992. Infiltration and Soil Water Movement. In: D. MAIDMENT, ed, *Handbook of hydrology*. McGraw-Hill Inc., .

RODRIGUEZ, F., CUDENNEC, C. and ANDRIEU, H., 2005. Application of morphological approaches to determine unit hydrographs of urban catchments. *Hydrological Processes*, **19**(5), pp. 1021-1035.

ROSSMAN, L.A., 2010. *Storm Water Management Model User's Manual - Version 5.0.* http://nepis.epa.gov/Exe/ZyPURL.cgi?Dockey=P100ERK4.txt edn. Cincinnati, OH: U.S. Environmental Protection Agency.

SAUNDERS, W., 1999. Preparation of DEMs for Use in Environmental Modeling Analysis, *1999 Esri User Conference*, 07/24 - 07/30 1999.

SCALENGHE, R. and MARSAN, F.A., 2009. The anthropogenic sealing of soils in urban areas. *Landscape and Urban Planning*, **90**(1–2), pp. 1-10.

SEMADENI-DAVIES, A., *Urban snowmelt processes–current research and modelling needs*. Lund, Sweden: Dept. Water Resources Engineering, Lund University.

SEUNA, P., KAUPPI, L., MELANEN, M. and KENTTÄMIES, K., 1986. Ihmisen toiminnan vaikutus hydrologiseen kiertoon. In: S. MUSTONEN, ed, *Sovellettu hydrologia*. Mänttä: Vesiyhdistys ry, pp. 387-420.

SMITH, D., LI, J. and BANTING, D., 2005. A PCSWMM/GIS-based water balance model for the Reesor Creek watershed. *Atmospheric Research*, **77**(1), pp. 388-406.

TEXAS DEPARTMENT OF TRANSPORTATION, 2011. *Hydraulic Design Manual.* Texas, USA: Texas Department of Transportation.

THIEKEN, A.H., LUECKE, A., DIEKKRUEGER, B. and RICHTER, O., 1999. Scaling input data by GIS for hydrological modelling. *Hydrological Processes,* **13**(4), pp. 611-630.

THIESSEN, A.H., 1911. Precipitation averages for large areas. *Monthly Weather Review,* **39**(7), pp. 1082-1089.

THOMPSON, D.B. and CLEVELAND, T.G., 2009. *Subdivision of Texas Watersheds for Hydrologic Modeling.* FHWA/TX -0–5822–01–2. Lubbock, Texas: Texas Tech University College of Engineering.

VAKKILAINEN, P., 1986. Haihdunta. In: S. MUSTONEN, ed, *Sovellettu hydrologia.* Mänttä: Vesiyhdistys ry, pp. 64-81.

VAKKILAINEN, P., SOVERI, J. and HARTIKAINEN, H., 1986. Maavedet. In: S. MUSTONEN, ed, *Sovellettu hydrologia.* Mänttä: Vesiyhdistys ry, pp. 82-100.

VALEO, C. and HO, C., 2004. Modelling urban snowmelt runoff. *Journal of Hydrology*, **299**(3), pp. 237-251.

VALTANEN, M., SILLANPÄÄ, N. and SETÄLÄ, H., 2013. Effects of land use intensity on stormwater runoff and its temporal occurrence in cold climates. *Hydrological Processes,* , pp. n/a-n/a.

VITO NV, 07/26/2012, 2012-last update, EUROLAND Product Catalogue [Homepage of Geoland2 consortium], [Online]. Available: http://www.geoland2.eu/portal/service/ShowServiceInfo.do?serviceId=D880A280&categoryId=D880A880 [01/28, 2013].

WOOLHISER, D.A., 1981. Physically Based Models of Watershed Runoff, V.P. SINGH, ed. In: *Rainfall-Runoff Relationship*, May 18-21 1981, Water Resources Publications, pp. 189--202.

ZHANG, H., WANG, Y., WANG, Y., LI, D. and WANG, X., 2013. The effect of watershed scale on HEC-HMS calibrated parameters: a case study in the Clear Creek watershed in Iowa, USA. *Hydrology and Earth System Sciences Discussions,* **10**, pp. 965-998.

ZOPPOU, C., 2001. Review of urban storm water models. *Environmental Modelling & Software,* **16**(3), pp. 195-231.

APPENDIX A – A Visual Basic script for calculating slope values cell-by-cell

```
Private Sub HydrologicalSlope()
    Dim RasterSizeX, RasterSizeY, i, j, i2, j2 As Integer
    Dim CellElevation, LowestNeighbour, HorizontalDifference, Slope As Double

    RasterSizeX = 1533
    RasterSizeY = 1769

    Sheets.Add.Name = "SlopeRaster"

    For i = 2 + 6 To RasterSizeX - 1 + 6
        For j = 2 To RasterSizeY - 1
            CellElevation = Sheets("km2_mm").Cells(i, j).Value
            HighestSlope = 0
            For i2 = -1 To 1
                For j2 = -1 To 1
                    NeighbourElevation = Sheets("km2_mm").Cells(i + i2, j + j2).Value
                    If NeighbourElevation < CellElevation Then
                        If i2 + j2 = -1 Or i2 + j2 = 1 Then
                            HorizontalDifference = 2
                        Else
                            HorizontalDifference = 2.8284271247
                        End If
                        Slope = (CellElevation - NeighbourElevation) / HorizontalDifference * 100
                        If Slope > HighestSlope Then
                            HighestSlope = Slope
                        End If
                    End If
                Next
            Next
            Sheets("SlopeRaster").Cells(i, j).Value = HighestSlope
        Next
    Next
End Sub
```